

**A dissertation entitled**

Harmonics and Instabilities in  
Thyristor Based Switching Circuits

submitted to the Graduate School of the  
University of Wisconsin-Madison  
in partial fulfillment of the requirements for the  
degree of Doctor of Philosophy

by

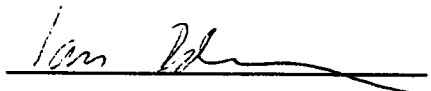
Sasan Ghombavani Jalali

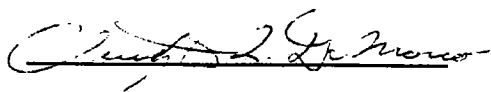
Degree to be awarded: December 1993    May 19\_\_    August 19\_\_

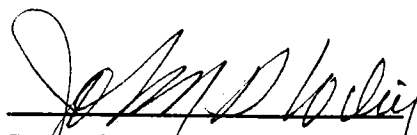
Approved by Dissertation Readers:

  
Major Professor

April 2, 1993  
Date of Examination





  
Dean, Graduate School

# HARMONICS AND INSTABILITIES IN THYRISTOR BASED SWITCHING CIRCUITS

Sasan Ghombavani Jalali

Under the supervision of Professor Robert H. Lasseter and  
Assistant Professor Ian Dobson at the University of Wisconsin-Madison

This thesis investigates nonlinear dynamics, harmonic distortions and bifurcation instabilities in thyristor switching circuits. The analysis is directed towards the study of a Thyristor Controlled Reactor (TCR) which consists of a fixed reactor and two oppositely poled thyristors. The dependence of the thyristor switching times on the system states causes the circuit nonlinearities and is the focus of much of the thesis. New concepts for instability, dynamic response and damping for TCR circuits are introduced. These concepts are general and can be extended to other switching circuits. Useful TCR circuit examples such as the 230 kV Kayenta advanced series compensator and the 230 kV Rimouski static Var system are used to numerically verify these concepts. We have found new instabilities in both the Kayenta and the Rimouski systems in which switching times change suddenly, or bifurcate as a system parameter varies slowly. Switching time bifurcations are associated with large distortions of the TCR current or voltage waveforms leading to a new earlier TCR current zero, the disappearance of a current zero, or a

## Acknowledgements

I would like to take this opportunity to thank my advisors, Professor Lasseter and Professor Dobson, for their patience and guidance throughout my doctoral studies.

My numerous meetings with Professor Lasseter helped me to define the problem and to keep in touch with the practical issues regarding it. Similarly, my numerous discussions with Professor Dobson provided me with the theoretical framework required in solving this problem.

The past three years of working together has given me the confidence to become an independent researcher, for which I am thankful.

Funding from EPRI under contracts RP 4000-29 and RP 8050-04 and from NSF PYI grant ECS-9157192 is gratefully acknowledged.

# Table of Contents

<b>1</b>	<b>Introduction</b>	<b>1</b>
<b>2</b>	<b>Thyristor Controlled Reactor (TCR)</b>	<b>8</b>
2.1	Two circuit examples using the TCR	10
2.2	Control methods and firing strategies	14
2.3	Summary	19
<b>3</b>	<b>Tools to Study the Thyristor Controlled Reactor</b>	<b>20</b>
3.1	Classical analysis	21
3.2	Average inductor model	24
3.3	Harmonic Admittance Methods	27
3.4	Nonlinear circuit dynamics of ASC	33
3.5	Time domain simulation	47
3.6	Summary	48
<b>4</b>	<b>Bifurcations, Harmonic Distortions and Resonance</b>	<b>49</b>
4.1	Resonance and harmonic distortions	49
4.2	Switching time bifurcation	51
4.3	Conventional and switching time bifurcations	54
4.4	Instabilities	55
4.5	summary	58
<b>5</b>	<b>Four TCR Circuit Examples Illustrating Bifurcation Instabilities</b>	<b>59</b>
5.1	The static VAR compensator	60

## List of Figures

1.1	Basic single phase TCR	1
1.2	Single phase line commutated converter	7
2.1	Basic single phase TCR	8
2.2	Classical operation of a TCR	9
2.3	Single phase static VAR system	10
2.4	Basic ASC circuit model	13
2.5	Control scheme for the TCR	14
2.6	Firing pulses using the equidistant firing scheme	16
2.7	The constant sigma controller	18
3.1	Single phase static VAR compensator	20
3.2	Advanced series compensator	20
3.3	Classical operation of a TCR	22
3.4	Classical method of computing $I_{\text{TCR}}(\omega t, \sigma)$ in a SVC	23
3.5	Classical method of computing harmonics in a SVC	23
3.6	Classical method of computing $V_{\text{TCR}}(\omega t, \sigma)$ in an ASC	24

5.5	Periodic orbits 4,5 and 6	65
5.6	Periodic solution 6 ( $\sigma \approx 56^\circ$ ) up to .3 seconds	66
5.7	Rimouski static VAR compensator	67
5.8	$\phi$ versus $\sigma$	69
5.9	The Kayenta ASC	70
5.10	Resonance predictions using the average inductor model	71
5.11	The fundamental and the 3rd harmonic of the TCR current	72
5.12	$\sigma_p$ steps down from $164^\circ$ to $160^\circ$	73
5.13	$\sigma_p$ steps up from $115^\circ$ to $120^\circ$	73
5.14	The fundamental and the 2nd component of the TCR current	75
5.15	Steady state operation at $\sigma_p \approx 140^\circ$	76
5.16	Loss of stability when ambient harmonics present	76
6.1	Single phase static VAR system	79
6.2	The circuit used to model the Jacobian DF in (6.1)	81
6.3	The simplest TCR circuit which illustrates damping ( $R=0$ )	82
6.4	TCR current in transient (dashed line) and steady state	83

7.9	DC current at point B	104
A.1	Thyristor controlled reactor	114
A.2	The switching function, $H(\omega t)$	115
B.1	Single phase line commutated converter	120
B.2	Switching functions	121
C.1	TCR harmonic current for (a and b) $L_r=1.7$ mH (c and d) $L_r=3.4$ mH and (d and e) $L_r=6.8$ mH	127
D.1	AC harmonics of the example 7.3 (a) current (b) voltage	129
D.2	DC harmonics of the example 7.3 (a) current (b) voltage	130

# Chapter 1

## Introduction

Over the last couple of years there has been significant activity in the development of Flexible AC Transmission Systems (FACTS). Much of this work has been directed towards advanced series compensation (ASC) systems based on a thyristor controlled reactor connected in parallel with a fixed capacitor [8,9,17,18,28]. This results in a controllable series impedance element for use in transmission systems. As static switching circuits such as FACTS proliferate, there is an increasing need to analyze and understand these circuits and their interactions with power systems. However, because of the dependence of the thyristor turn on and off times on the system states, thyristor switching circuits are nonlinear and very awkward to analyze using standard mathematical techniques [17,25].

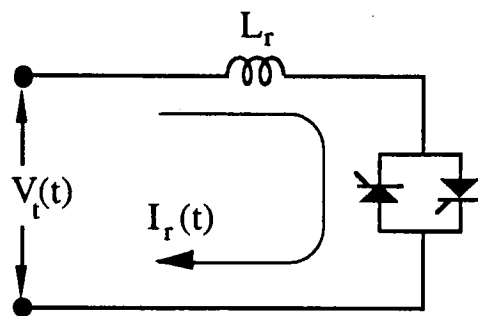


*Figure 1.1. Basic single phase TCR*

This thesis will use the Thyristor Controlled Reactor (TCR) circuit shown in the Figure 1.1 as an illustrative example for study. This circuit is a good choice for developing new techniques of analysis since the number of switching elements is small. Two useful TCR circuits are the



associated with the thyristor switching times, it is still one of the most common methods of computing eigenvalues [11,16,23,33]. We have found the average inductor model very useful in approximately predicting potential resonance points.

4) The dynamics of a switching circuits may be studied using state space averaging. It can be shown that averaging the state space equations is a good approximation for the pulse-width modulated convertors [34]. On the other hand, it can give incorrect results for the naturally commutated circuits such as the resonant link convertors or the TCR circuits. Sanders in [39] extends this method to study the convertors which switch at lower frequencies by adding higher order correction terms to the classical formulation. However, it is not clear how this method can be used to study circuits with discontinuous modes of operation such as the thyristor controlled reactor.

5) The nonlinear dynamics of a TCR circuit were studied using the Poincare mapping from the dynamical systems theory [20,46]. In this approach, the system state is strobed at discrete times which are spaced by one period of the fundamental frequency,  $T$  and the system is studied by means of the Poincare map. The Poincare map advances the system state from one discrete time to the system state at the next discrete time. If the circuit has a steady state solution of period  $T$ , then the Poincare map has a fixed point. Except for marginal cases, the Poincare map can be differentiated and a formula for its Jacobian can be obtained. The Jacobian of the Poincare map evaluated at the fixed point can be used to

6) The harmonics of a power system which include a three phase thyristor bridge may be computed using the harmonic power flow method [51,52]. In this method, the AC current flowing into the converter terminal is solved in terms of the convertor AC voltage. One of the drawbacks is that the DC load is assumed to be a series combination of a resistor, inductor and a DC source. Another drawback is that the harmonic interactions of the converter and power system can not be studied when ambient even harmonics are present.

7) Peter Wood in [50] introduced the switching function method to compute the harmonics generated by converters which have fixed switching times. Bohmann and Lasseter extended this method to TCR circuits [7]. By expressing the TCR voltage and current as a Fourier series, a TCR harmonic admittance matrix is constructed. The admittance matrix is then incorporated into a power system providing a quick and general method to compute the power system harmonics. This method is explained in detail in chapter 3 and is used in chapter 5 to compute the harmonics of TCR circuits.

Classical analysis is often applicable, but can as demonstrated in this thesis and in [7,9] fail for certain circuit parameters and operating conditions. Under these conditions, both the voltage and the current waveforms become greatly distorted with large harmonic components. This phenomena is due to the circuit operating close to its resonance point and can be detected by the eigenvalues of the half wave Poincare map being -1.

coupling matrix which illustrates the coupling between the convertor voltage and current harmonics is developed. It is shown how this matrix can be incorporated into a power system and how the power system harmonics can be accurately calculated. In addition, an example system which exhibits large harmonic distortions and switching time bifurcation is also presented. In particular, it is shown that there may be two steady state solutions and/or no solutions over the regions for which the classical method predicts both the existence and the uniqueness of the solution.

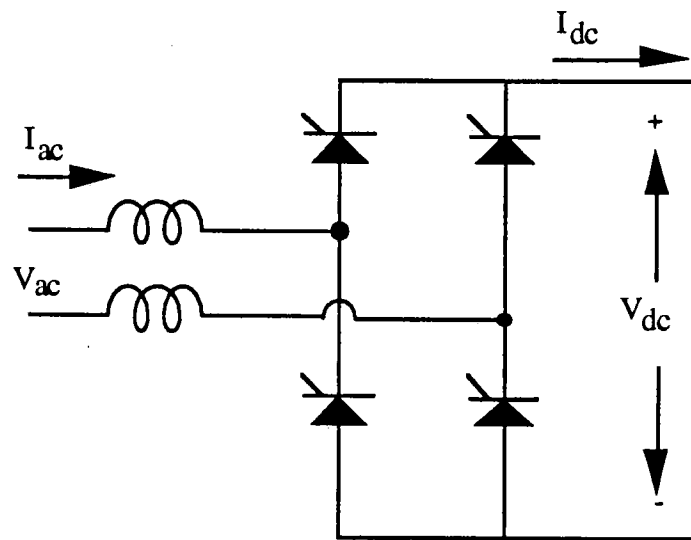


*Figure 1.2 Single phase line commutated converter*

## Chapter 2

### Thyristor Controlled Reactor (TCR)

Thyristor controlled reactors are typically composed of back to back thyristors used to vary the duty cycle of an inductor. In periodic steady state, the effect of the 60 Hz fundamental is to absorb varying amounts of reactive power from a power system network. Figure 2.1 shows a basic single phase Thyristor Controlled Reactor (TCR). It consists of a fixed reactor of inductance  $L$  (usually air core) and two oppositely poled thyristors which conduct on alternate half cycles of the supply frequency.

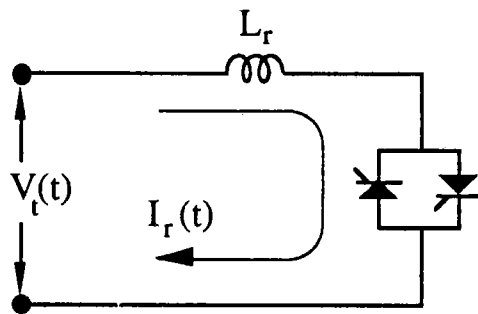


*Figure 2.1. Basic single phase TCR*

A thyristor conducts current only in the forward direction, can block voltage in both directions, turns on when a firing signal is provided and turns off after a current zero. The currently available thyristors can block a voltage range between 4000 to 6000 volts and can carry a current ranging from 2000 to 4000 amperes. In general, between 10 to 40 thyristor valves are connected in series to meet the required blocking voltage levels [21].

## 2.1 Two circuit examples using TCR

To illustrate some of the potential problems associated with the operation of TCR switching circuits and methods developed in this report, this section introduces two commonly used TCR circuits. These circuits are a single phase static VAR compensator and a single phase advanced series compensator.

### *The Static Var Compensator (SVC)*

Figure 2.3 shows a SVC consisting of a thyristor controlled reactor (TCR) and a parallel capacitor. This system is connected to an infinite bus behind a power system impedance of an inductance  $L_s$  and a resistance  $R_s$  in series. The controlled reactor is modelled as a series combination of an inductor  $L_r$  and  $R_r$ .

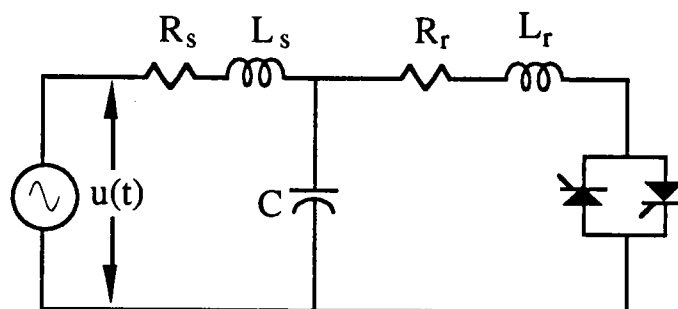


*Figure 2.3. Single phase static VAR system*

The above circuit can provide leading to lagging reactive power to the AC system. This characteristic behavior of the 60 Hz fundamental is approximately equivalent to an ideal system voltage source at the point of connection except that it has a limited range in which the voltage can be controlled.

been directed towards advanced series compensation (ASC) systems based on a thyristor controlled reactor connected in parallel with a fixed capacitor. This results in a controllable series impedance element for use in transmission systems.

Currently there are three such systems in various stages of commercialization. The Kanayna River system, West Virginia, is a joint R&D effort by American Electric Power Service Corporation and Asea Brown Boveri. This FACTS controller has been recently commissioned [32]. The system was planned to have 788 Mvar of series capacitance or 60% compensation. In the first phase of the project a prototype thyristor control module has been installed across one phase of 131 Mvar of compensation to create an ASC system. The remaining two phases will be installed following successful testing of this unit.

Western Area Power Administration is installing a 230 kV, 330 Mvar ASC system in northeastern Arizona at Kayenta Substation [8]. This system is supplied by Siemens AG. This scheme is comprised of 285 Mvar of conventional series capacitor banks with the remaining 45 Mvar of capacitance controlled by a parallel thyristor controlled reactor. Implementation of this FACTS scheme has progressed through the equipment development phases and currently is being installed at the site.

A third scheme is a major Electric Power Research Institute project with General Electric to develop a thyristor controlled series capacitor. A second phase of this project is to install such a system on a 500 kV transmission line in the Bonneville Power Administration region. This

## 2.2 Control methods and firing strategies

This section discusses the basic control issues and various firing schemes which are used to operate the TCR circuits.

### *Basic control scheme*

Figure 2.5 shows a basic TCR control scheme with three function blocks. The first is the interface block which computes the root mean square of the TCR voltage. The second block is the regulator block. The input to this block is the difference between the reference quantities  $V_{ref}$  and the measured quantities  $V_{rms}$  and the output is a request value for either the thyristor conduction time  $\sigma$  or the firing delay  $\alpha$ . The third block, the gate pulse generator, generates the firing pulses for the thyristors. The gate pulse generator usually uses one of the synchronization schemes described below so as to achieve the requested  $\sigma$  or  $\alpha$ .

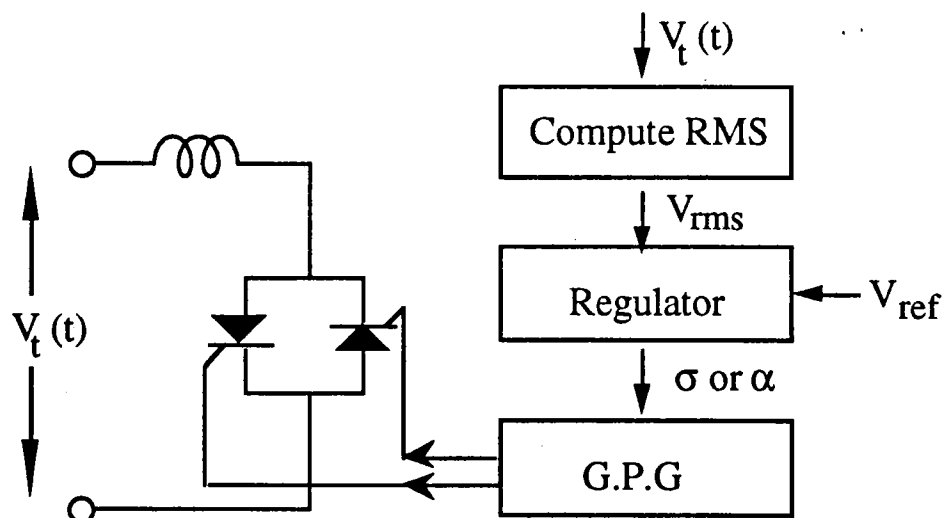
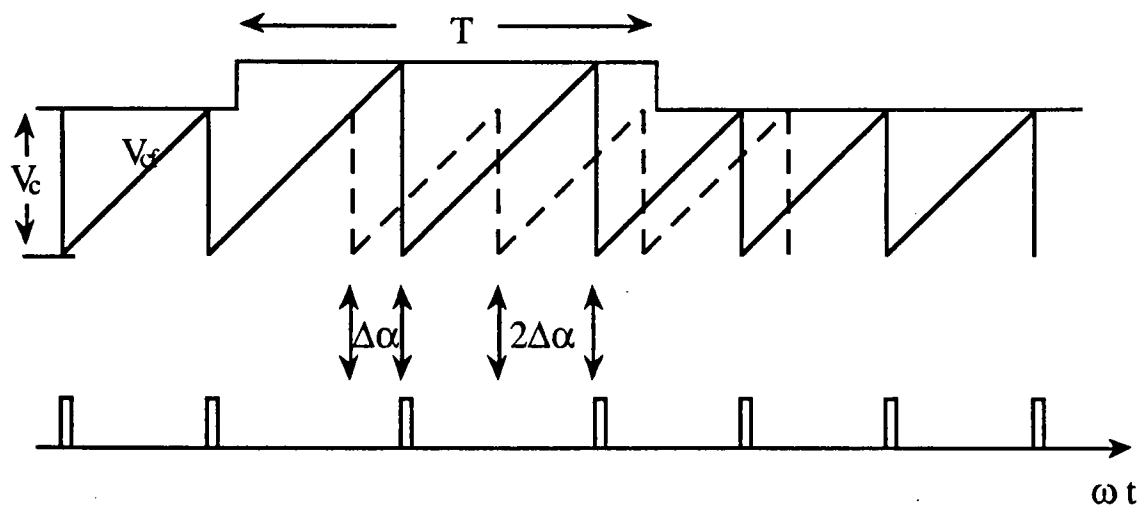


Figure 2.5. Control scheme for the TCR

parameter  $V_c$ . The phase of the equally spaced firing pulses has some arbitrary value with respect to the voltage across the TCR. In practice, this phase would drift relative to the TCR voltage. This is usually corrected by an external negative feedback loop.

An alternative to the phase locked loop scheme is shown in Figure 2.6 [4]. In this method, the firing pulses are sent whenever the integrator function  $V_{cf}$  intersects the controller output voltage  $V_c$ . At this point, the integrator  $V_{cf}$  is reset and the integration process starts again. The integrator function and the controller output voltage are chosen such that the firing pulses are spaced by 180 electrical degrees so that there are two firing pulses per cycle.



*Figure 2.6. Firing pulses using the equidistant firing scheme*

Figure 2.6 illustrates how the relative phase of the firing pulses can be changed by temporarily varying the control signal  $V_c$ . Let us assume that the firing pulses have initially a delay angle  $\alpha$  with respect to the actual system. As long as the controller output voltage is fixed,  $\alpha$  is also fixed



conduction and 1.0 when conduction. Integrating this signal results in an output which exhibits a slope change at the point where conduction stops. The output of the integrator is negatively biased by a constant value of  $2\pi$  as shown in the Figure 2.7c. This signal is input to a zero plus detector which issues the firing pulses whenever the signal becomes positive. The resulting firing pulses are shown in the Figure 2.7d.

The main advantage of this scheme is that there is no need for accurate measurement of either voltage or current.

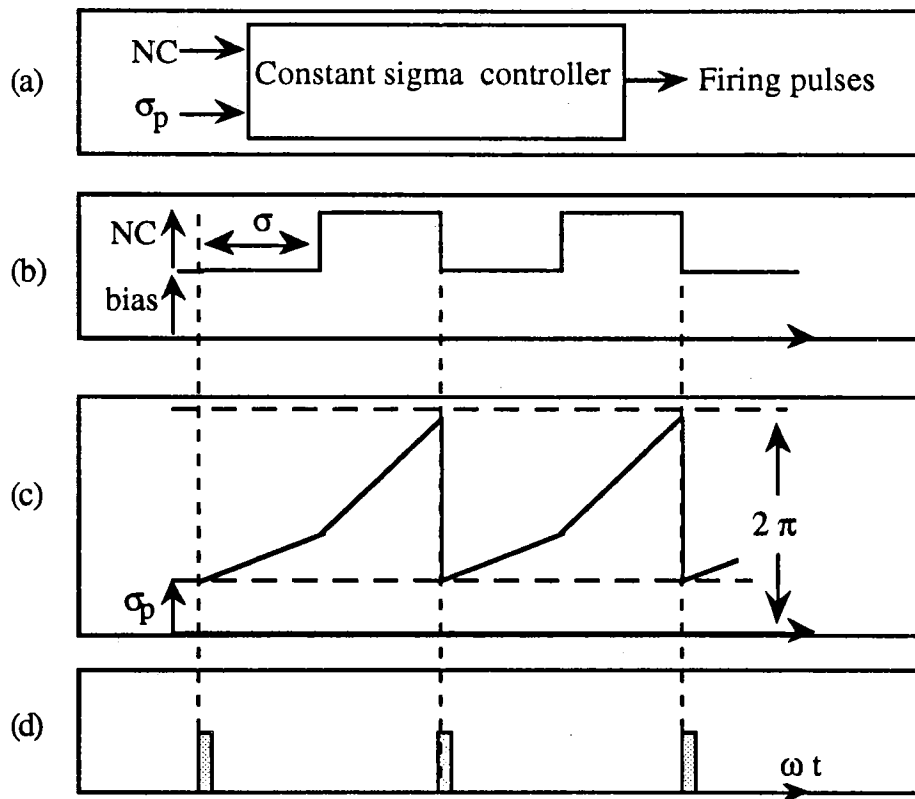


Figure 2.7. The constant sigma controller

## Chapter 3

### Tools to Study the Thyristor Controlled Reactor

A thyristor controlled reactor (TCR) is a thyristor based compensator which is capable of absorbing reactive power from a power system network. In chapter 2, issues associated with the control and operation and firing strategies for two useful TCR circuits were studied. These two TCR circuits are, the Static Var Compensator (SVC) and the Advanced Series Compensator (ASC) shown in Figures 1 and 2.

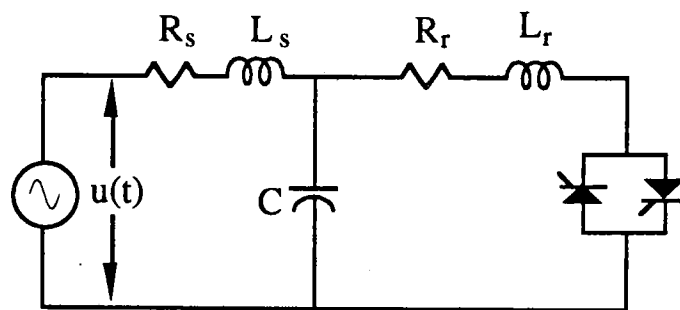


Figure 3.1. Single phase static VAR compensator

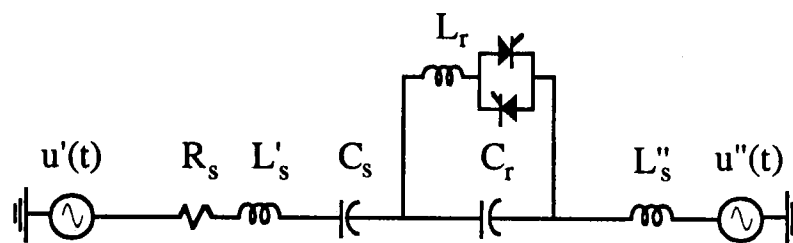


Figure 3.2. Advanced series compensator

In section 3.1, the classical method of computing the system harmonics is explained. Section 3.2 introduces a simple average inductor model useful in approximately predicting potential problems with the operation

shown by the gray line in the Figure 3.3. In the classical analysis, the two variables  $\sigma$  and  $\alpha$  are commonly used in explaining the TCR operation.  $\sigma$  denotes the conduction time of a thyristor while  $\alpha$  is the firing point relative to the voltage across the thyristor. These two variables are related by  $2\alpha + \sigma = 2\pi$ . Therefore, if the thyristors are fired at the point where the TCR voltage is at a peak, ( $\alpha = \pi/2$ ), full conduction results ( $\sigma = \pi$ ). If the firing is delayed from the peak voltage, the current becomes discontinuous with a reduced fundamental component of reactive current. This partial conduction is obtained with firing angles between 90 and 180 electrical degrees.

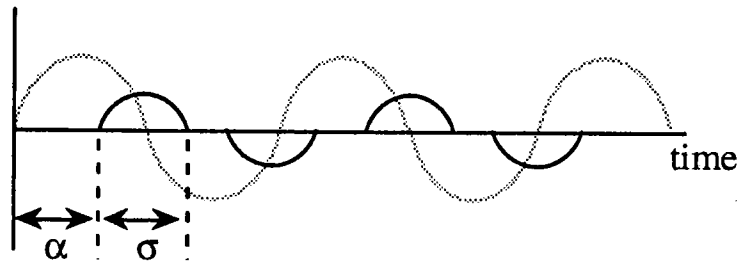


Figure 3.3. Classical operation of a TCR

The classical analysis provides a two step process by which the power system harmonics can be computed as described below.

### *Harmonics in a static VAR compensator*

First the TCR is modelled as an equivalent harmonic current source:

$$I_{\text{tcr}}(\omega t, \sigma) = \sum_{n=1}^{n=\infty} I_n(\sigma) e^{jn\omega t} \quad (3.1)$$

$$V_{\text{tcr}}(\omega t, \sigma) = \sum_{n=1}^{n=\infty} V_n(\sigma) e^{jn\omega t} \quad (3.2)$$

where  $V_n(\sigma)$  is the  $n$ th harmonic of  $V_{\text{tcr}}(\omega t, \sigma)$ . To compute  $V_{\text{tcr}}(\omega t, \sigma)$ , the AC system as seen from the TCR terminals is replaced by a Thevenin current source  $I_{\text{th}}(\omega t)$  in parallel with a Thevenin capacitance  $C_{\text{th}}$  as shown in the Figure 3.7 [8,9].

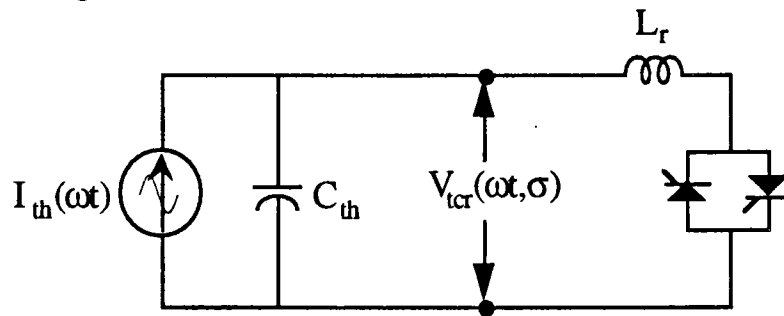


Figure 3.6. Classical method of computing  $V_{\text{tcr}}(\omega t, \sigma)$  in an ASC

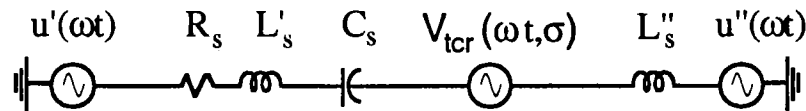


Figure 3.7. Classical method of computing harmonics in an ASC

Power system harmonics are then calculated by replacing the TCR and  $C_r$  with  $V_{\text{tcr}}(\omega t, \sigma)$  as shown in the Figure 3.5. This method ignores the important harmonic interaction between the TCR and the power system.

### 3.2 Average inductor model

The average inductor model is a simple and useful method in approximately predicting potential problems with the operation of a TCR. In this model, the TCR is represented as a variable inductance

The harmonic resonant frequency of the system can be computed from the above equivalent model as:

$$f_{\text{res}} = \frac{1}{2\pi} \sqrt{\frac{1}{C L_s} + \frac{1}{C L_{\text{eq}}(\sigma)}} \quad (3.4)$$

Equation (3.4) implies that the static var system harmonic resonance frequency depends on the conduction time,  $\sigma$ , of the TCR and the inductive and capacitive components. For example, typical values of system inductance, fixed capacitor and variable inductance can have resonance at the 5th harmonic. In this case, this model predicts that the system experiences large harmonic voltages and currents.

### *Advanced series compensator*

Figure 3.9 shows the application of the average inductor model to the advanced series compensator example with all the circuit resistances are ignored.

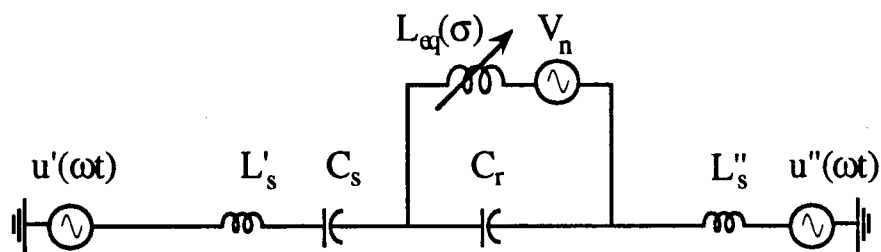


*Figure 3.9. Modelling the ASC with an average inductor model*

The resonant frequency of this system can be computed from the above equivalent model and is given by:

$$f_{\text{res}} = \frac{1}{2\pi} \sqrt{A + \sqrt{A^2 - \frac{1}{C_r C_s L_s L_{\text{eq}}(\sigma)}}} \quad (3.5)$$

The switching function,  $H(\omega t)$ , shown in Figure 3.11 has a value of one whenever a thyristor is on and zero when the thyristors are off. Since a thyristor turns off when its current goes through zero, the conduction time,  $\sigma$  depends on the turn on time  $\phi$ , the terminal voltage  $V_t(\omega t)$  and the TCR reactance  $L_r$ . Therefore the switching function is dependent on the terminal voltage through the turn on/off time of the thyristors.

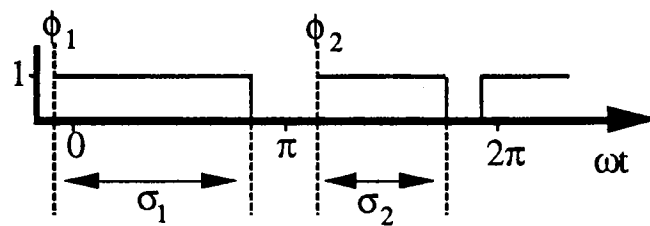


Figure 3.11. The switching function,  $H(\omega t)$

The voltage across the TCR inductance  $V_r(\omega t)$  is the product of the switching function  $H(\omega t)$  by the terminal voltage  $V_t(\omega t)$ . Assuming periodicity, the Fourier components of  $H(\omega t)$ ,  $V_t(\omega t)$  and  $V_r(\omega t)$  are related by the matrix equation (for details see the appendix A ):

$$\begin{bmatrix} \cdot \\ \cdot \\ v_{r-3} \\ v_{r-2} \\ v_{r-1} \\ \cdot \\ \cdot \end{bmatrix} = \begin{bmatrix} \cdot & \cdot & \cdot & \cdot & \cdot & \cdot & \cdot \\ \cdot & \cdot & \cdot & \cdot & \cdot & \cdot & \cdot \\ \cdot & \cdot & h_0 & h_{-1} & h_{-2} & \cdot & \cdot \\ \cdot & \cdot & h_1 & h_0 & h_{-1} & \cdot & \cdot \\ \cdot & \cdot & h_2 & h_1 & h_0 & \cdot & \cdot \\ \cdot & \cdot & \cdot & \cdot & \cdot & \cdot & \cdot \\ \cdot & \cdot & \cdot & \cdot & \cdot & \cdot & \cdot \end{bmatrix} \begin{bmatrix} \cdot \\ \cdot \\ v_{t-3} \\ v_{t-2} \\ v_{t-1} \\ \cdot \\ \cdot \end{bmatrix} \quad (3.6)$$

where  $h_n$  is a function of  $\sigma_1, \phi_1, \sigma_2$  and  $\phi_2$ . The above matrix equation illustrates the coupling between the harmonics which is an important

bus connecting the TCR to the external system as shown in Figure 3.12. Without the TCR connected, the resulting linear system has a harmonic  $Z_{th}$  matrix.

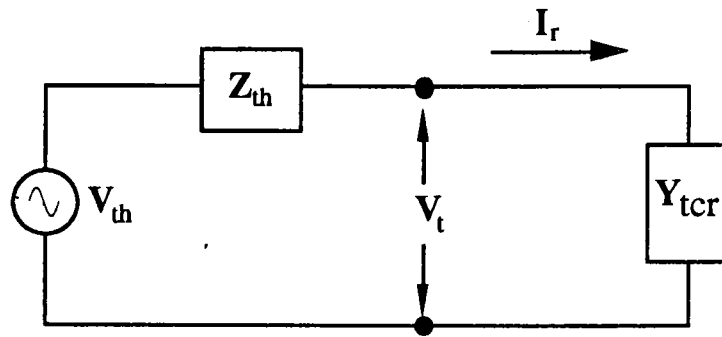


Figure 3.12. The reduced equivalent system

The equivalent system impedance is the diagonal element of the  $Z_{th}$  matrix corresponding to the TCR bus. In the equivalent system shown the voltage across the terminals is:

$$V_t = V_{th} - Z_{th} I_r \quad (3.10)$$

Using  $I_r$  given in equation (3.9) allows an expression for  $V_t$  to be written. ( $I$  is the identity matrix)

$$V_{th} = [ I + Z_{th} Y_{tcr}(\sigma_1, \phi_1, \sigma_1, \phi_1) ] V_t \quad (3.11)$$

The zero thyristor current at the switching times  $(\phi_1 + \sigma_1)$  and  $(\phi_2 + \sigma_2)$  define two relationships between the times  $\sigma_1$ ,  $\phi_1$ ,  $\sigma_2$  and  $\phi_2$  and the terminal voltage harmonics as derived in the appendix A. These are:

$$0 = v_{t0} \sigma_i + \sum_{m=-\infty}^{\infty} \frac{v_{tm}}{jm} [ e^{-jm(\phi_i + \sigma_i)} - e^{-jm\phi_i} ] \quad \text{for } i=1,2 \quad (3.12)$$

Rewriting the above equations yields the following two relationships between the thyristor switching times.

$$\sigma_{\text{req}} = \frac{\sigma_1 + \sigma_2}{2} \quad (3.16)$$

$$\phi_2 - \phi_1 = \pi + \frac{\sigma_1 - \sigma_{\text{req}}}{2} \quad (3.17)$$

The control parameter  $\sigma_{\text{req}}$  takes a value from 0 to  $\pi$  where  $\sigma_{\text{req}}$  is a given control point. Equations (3.11) and (3.12) together with (3.16) and (3.17) give us a complete set of equations to solve for the periodic solutions of the system under the constant sigma controller. Note that if the periodic solution is half wave symmetric we have  $\sigma_1 = \sigma_2 = \sigma_{\text{req}}$  otherwise,  $\sigma_{\text{req}}$  represents the average of the two conduction lengths. The suggested solution algorithm is to use the Newton's method as was done earlier for the equidistant firing controller. For initial guess, one may solve (3.11) for  $V_t$  by choosing  $\sigma_1 = \sigma_2 = \sigma_{\text{req}}$ ,  $\phi_2 = \phi_1 + \pi$  and

$$\phi_1 = \pi - \frac{\sigma_{\text{req}}}{2} \quad (3.18)$$

Computation with the infinite harmonic system vectors and matrices are made by assuming the higher harmonic terms can be neglected. From the details in the appendix, it is seen that the elements in the switching matrix  $\mathbf{H}$ , which defines  $\mathbf{Y}_{\text{tcr}}$  fall off as  $1/n$ . The harmonics in power systems will generally do the same. This allows the higher harmonics to be ignored. The vectors and matrices can therefore be truncated at a harmonic number above the harmonics of interest.



A thyristor conducts current only in the forward direction, can block voltage in both directions, turns on when a firing signal is provided and turns off after a current zero. The thyristors are assumed ideal so that the nonlinearity of the circuit only arises from the dependence of the switch on and off times of the thyristors on the system state.

During the thyristor conduction time, the system state vector  $x(t)$  specifies the TCR current, voltage, the line current and the fixed series capacitor voltage:

$$x(t) = \begin{bmatrix} I_r(t) \\ V_r(t) \\ I_s(t) \\ V_s(t) \end{bmatrix} \quad (3.19)$$

The system input  $u(t)=u'(t)-u''(t)$  is the net source voltage which is assumed to be periodic with period  $T$  and the system dynamics are described by the following set of linear differential equations:

$$\dot{x}(t) = Ax(t) + Bu(t) \quad (3.20)$$

where

$$A = \begin{bmatrix} 0 & 1/L_r & 0 & 0 \\ -1/C_r & 0 & 1/C_r & 0 \\ 0 & -1/L_s & -R_s/L_s & -1/L_s \\ 0 & 0 & 1/C_s & 0 \end{bmatrix} \text{ and } B = \begin{bmatrix} 0 \\ 0 \\ 1/L_s \\ 0 \end{bmatrix} \quad (3.21)$$

During the off time of each thyristor, the circuit state is constrained to lie in the plane  $I_r=0$  of zero thyristor current. In this mode, the system

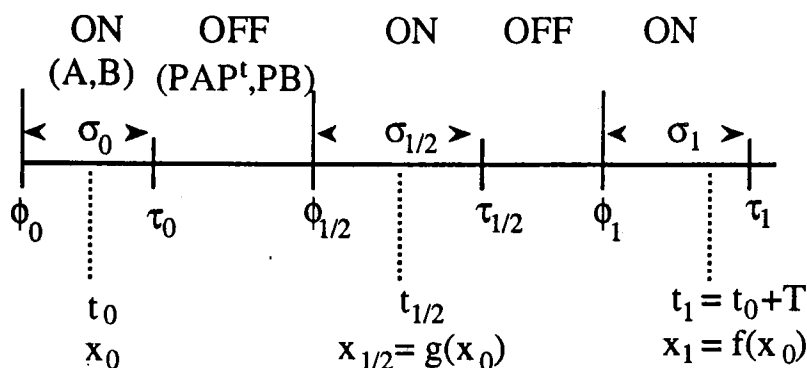


Figure 3.14. ASC system dynamics from time  $\phi_0$  to  $\tau_1$ .

The thyristor turn on times at  $\phi_{1/2}$  and  $\phi_1$  depend on the firing scheme and the closed loop control. We study the open loop system when operated with one of the four common firing schemes. These are equidistant firing, constant sigma controller and synchronization on the ASC voltage or the ASC line current.

(a) In equidistant firing the thyristor turn on pulses are supplied periodically and the system is controlled by varying the phase of the firing pulses,  $\phi$ . Since the relationship between  $\phi$  and the TCR firing angle  $\alpha$  depends on the line impedance, a negative feed back loop modifying  $\phi$  is usually used to ensure a requested  $\alpha$ . In this section, we restrict our analysis to an equidistant firing with no feed back control i.e., the thyristor turn on times are computed using a requested phase delay  $\phi_{req}$  as follows:

$$\phi_{1/2} = \frac{T}{2} + \phi_{req} \quad (3.25)$$

$$\phi_1 = T + \phi_{req} \quad (3.26)$$

$$\phi_1 = \alpha_{\text{reqc}} + \tau_{c1/2} \quad (3.32)$$

The state at the switch on time  $\phi_0$  is denoted either by the vector  $y(\phi_0)$  or by the vector  $x(\phi_0)$ . These representations of the state at the switch on time are related by

$$x(\phi_0) = P^t y(\phi_0) \quad (3.33)$$

Equation (3.33) expresses the fact that the state in  $x$  coordinates at a switch on is computed from the  $y$  coordinates by adding a first component which has value zero. The state at the switch off time  $\tau_0$  is similarly denoted either by  $x(\tau_0)$  or  $y(\tau_0)$  and these are related by

$$y(\tau_0) = P x(\tau_0) \quad (3.34)$$

The matrix  $P$  in equation (3.34) may be thought of as projecting the vector  $x$  onto the hyperplane of zero thyristor current. Given a time interval  $[s_1, s_2]$ , it is convenient to write  $f(., s_1, s_2)$  for the map which advances the state at  $s_1$  to the state at  $s_2$ . For example, a Poincare map which advances the state by one period  $T$  starting at time  $t_0$  may be written  $f(x, t_0, t_0 + T)$ . For convenience, we adopt the notation that when the thyristor is on during all of the time interval  $[s_1, s_2]$ , we write  $f(x, s_1, s_2)$  as  $f_{\text{on}}(x, s_1, s_2)$ . Similarly, if the thyristor is off during  $[s_1, s_2]$ , we write  $f(y, s_1, s_2)$  as  $f_{\text{off}}(y, s_1, s_2)$ .  $f_{\text{on}}$  or  $f_{\text{off}}$  can be computed by integrating the linear system (3.20) or (3.23) over the corresponding time intervals.

$$f(x_0, t_0, t_{1/2}) = f_{\text{on}}(P^t f_{\text{off}}(P f_{\text{on}}(x_0, t_0, \tau_0), \tau_0, \phi_{1/2}), \phi_{1/2}, t_{1/2}) \quad (3.39)$$

The Poincare map may now be written by composing two successive half cycle maps and then neglecting the gory details of the time arguments:

$$f(x_0, t_0, t_0+T) = f_{\text{on}} P^t f_{\text{off}} P f_{\text{on}} P^t f_{\text{off}} P f_{\text{on}} x(t_0) \quad (3.40)$$

We assume that gradient of the thyristor current as it turns off is negative so that the Poincare map is smooth and differentiable.

### *Important Simplification*

Let  $[s_1, s_2]$  be a fixed time interval including a thyristor turn off at time  $\tau$  and no other switchings. For convenience, let  $x_1$  express the state at time  $s_1$ . Define  $H(x_1, \tau)$  as:

$$\begin{aligned} H(x_1, \tau) &= f_{\text{off}}(P f_{\text{on}}(x_1, s_1, \tau), \tau, s_2) = \\ &= e^{PAP^t(s_2-\tau)} P e^{A(\tau-s_1)} \left[ x_1 + \int_{s_1}^{\tau} e^{A(s_1-\alpha)} B u(\alpha) d\alpha \right] + \int_{\tau}^{s_2} e^{PAP^t(s_2-\alpha)} P B u(\alpha) d\alpha \end{aligned} \quad (3.41)$$

Note that  $H$  expresses  $y(s_2)$  as a function of  $x_1$  and the switch off time  $\tau$ .  $\tau$  is a function of  $x_1$  which is determined by the constraint of zero thyristor current at time  $\tau$ . The map  $f(x_1, s_1, s_2)$  which advances the state  $x_1$  to the state  $y(s_2)$  is equal to:

$$f(x_1, s_1, s_2) = H(x_1, \tau(x_1)) \quad (3.42)$$

The chain rule gives:

Despite the simplification, it is sometimes necessary to compute  $D\tau$ . The equation which determines the thyristor turn off time  $\tau$  is the first positive root of:

$$0 = c\dot{x}(\tau) = ce^{A(\tau-s_1)} \left[ x_1 + \int_{s_1}^{\tau} e^{A(s_1-\alpha)} Bu(\alpha) d\alpha \right] \quad (3.47)$$

where  $c=(1,0,0,0)$ . Differentiation with respect to  $s_1$  and solving for  $D\tau$  yields:

$$D\tau = \frac{-ce^{A(\tau-s_1)}}{c(Ax(\tau) + Bu(\tau))} = \frac{-ce^{A(\tau-s_1)}}{c\dot{x}(\tau-)} \quad (3.48)$$

Note that  $c\dot{x}(\tau-)$  (the limit of  $c\dot{x}(t)$  as  $t$  approaches  $\tau$  from below) is the gradient of the thyristor current as it turns off at  $\tau$ .

### *Jacobian and stability*

When the ASC is in steady state with a periodic trajectory of period  $T$ , the Poincare map has a corresponding fixed point. That is,

$$f(x(t_0), t_0, t_0+T) = x(t_0) \quad (3.49)$$

The stability of a periodic orbit is the same as the stability of the corresponding fixed point of the Poincare map [6,7]. That is, the stability of the periodic orbit can be computed from the Jacobian of the Poincare map evaluated at the fixed point. In particular, the periodic orbit is exponentially stable if the eigenvalues of the Jacobian lie inside the unit circle. Since the thyristor turn off time and the Poincare map

$$\frac{\partial H_0}{\partial \phi_{1/2}} = -e^{(t_{1/2} - \phi_{1/2})} c^t c \dot{x}(\phi_{1/2} +) \quad (3.55)$$

where  $c \dot{x}(\phi_{1/2} +)$  is the gradient of the TCR current as it turns on at  $\phi_{1/2}$ . In (3.53), the row vector  $D\phi_{1/2}$  is the gradient of the turn on time  $\phi_{1/2}$  with respect to  $x_0$ . This term depends on the firing scheme as follows:

a) In an equidistant firing,  $\phi_{1/2} = (T/2) + \phi_{req}$  as given in (3.25). Hence  $D\phi_{1/2} = 0$ . This is the simplest firing scheme i.e. the turn on time does not depend on the system state.

b) In the constant sigma controller,  $\phi_{1/2} = (\phi_0 + \tau_0 + 2\pi - \sigma_{req})/2$  as given in (3.27).  $\phi_0$  and  $\tau_0$  are the previous turn on and turn off times. Both are dependent on  $x_0$ . Differentiation yields:

$$D\phi_{1/2} = \frac{D\phi_0 + D\tau_0}{2} \quad (3.56)$$

where  $D\phi_0$  and  $D\tau_0$  represent the gradient of the turn on time  $\phi_0$  and turn off time  $\tau_0$  with respect to  $x_0$ . By analogy with (3.48),  $D\tau_0$  and  $D\phi_0$  are equal to:

$$D\tau_0 = \frac{-ce^{A(\tau_0 - t_0)}}{c \dot{x}(\tau_0 -)} \quad (3.57)$$

$$D\phi_0 = \frac{-ce^{A(\phi_0 - t_0)}}{c \dot{x}(\phi_0 +)} \quad (3.58)$$

where  $c = (1, 0, 0, 0)$ , and the terms in the denominator denote the gradients of the TCR current as it turns on at  $\phi_0$  and turns off at  $\tau_0$ .

Note that  $H_{1/2}$  expresses  $x(t_1)$  as a function of  $x_{1/2}$ , the turn off time  $\tau_{1/2}$  and the turn on time  $\phi_1$ .  $\tau_{1/2}$  is a function of  $x_{1/2}$  which is determined by the constraint of zero thyristor current at time  $\tau_{1/2}$ . The turn on time  $\phi_1$  may or may not depend on  $x_{1/2}$  depending on the firing strategy. Then the second half cycle map  $f(x_{1/2}, t_{1/2}, t_1)$  is equal to:

$$f(x_{1/2}, t_{1/2}, t_1) = H_{1/2}(x_{1/2}, \tau_{1/2}(x_{1/2}), \phi_1(x_{1/2})) \quad (3.62)$$

Using the chain rule and the simplification, the  $Df(x_{1/2}, t_{1/2}, t_1)$  is equal to:

$$Df(x_{1/2}, t_{1/2}, t_1) = \frac{\partial H_{1/2}}{\partial x_{1/2}} + \frac{\partial H_{1/2}}{\partial \phi_1} D\phi_1 \quad (3.63)$$

where each term in the right hand side can directly be written from its corresponding term as defined in the equations (3.53) to (3.60) by replacing all the subscripts "1/2" by "1" and the subscripts "0" by "1/2". Next, using the chain rule, the Jacobian of the Poincare map is given by:

$$Df(x_0, t_0, t_1) = Df(x_{1/2}, t_{1/2}, t_1) Df(x_0, t_0, t_{1/2}) \quad (3.64)$$

where  $Df(x_{1/2}, t_{1/2}, t_1)$  and  $Df(x_0, t_0, t_{1/2})$  are given by (3.53) and (3.63).

### *Simplifications for symmetric periodic orbits*

It is convenient to take advantage of symmetry when the periodic orbits are half wave symmetric. Half wave symmetry of a periodic orbit means that the system states are equal in magnitude and opposite in sign to the

quantitative method which provides little understanding of the important interactions.

Lasseter has shown how the ElectroMagnetic Transient Program (EMTP) [10] can be used to simulate TCR switching circuits using different firing strategies. In particular, it is shown how the constant sigma controller firing strategy can be modelled through the EMTP. All of the time domain simulations in this report are done using the EMTP as the simulation program.

### **3.6 Summary**

Both conventional and novel tools for studying TCR circuits were discussed. Frequency plane analysis suffers from the simplification required to achieve a solution. Section 3.3 describes how Fourier techniques can be used to construct a TCR harmonic admittance matrix. The admittance matrix can then be incorporated into a power system providing a quick method to calculate system harmonics. Section 3.4 studies the nonlinear circuit dynamics of an advanced series compensator using the Poincare mapping from dynamical systems theory. It is shown how the thyristor turn off time may be regarded as a fixed turn off time when deriving the system Jacobian. This fact results in a simple and useful formula for the Jacobian matrix of the Poincare map when the TCR is operating with an equidistant firing. It is also shown how correction terms may be added to the simple formula to compute the Jacobian matrix when the TCR is operating with other firing schemes.



## Chapter 4

### **Bifurcations, Harmonic Distortions and Resonance**

The classical analysis is often applicable, but can fail for certain circuit parameters and operating conditions. Under these conditions, the TCR current and voltage waveforms can become highly distorted. These large harmonic distortions are associated with the natural frequencies of the circuit, from when the reactor is fully on to when it is fully off, spanning an odd harmonic number. Section 4.1, discusses the large harmonic distortions to the circuit operating close to its resonance point. It is shown how this resonance point may be predicted through the computation of the eigenvalues. The large harmonic distortions can lead to instabilities associated with either a new earlier TCR current zero, the disappearance of the TCR current zero or a thyristor misfire (section 4.2). These instabilities, called switching time bifurcations, are very different from conventional bifurcations in that they are not detected by the eigenvalues the Jacobian matrix crossing the unit circle. However, different firing schemes can introduce conventional bifurcations just before a switching time bifurcation (section 4.4).

#### **4.1 Resonance and harmonic distortions**

Lasseter and Bohmann showed that a single phase SVC circuit can exhibit behavior much like resonance in a linear circuit for certain parameter values [7]. In particular, resonance is expected when the resonant frequency of the circuit from when the TCR is fully on to when it is fully

3.4).  $g(\cdot)$  is a bounded function with terms involving the integration of the input over the period. Rewriting (4.3) as:

$$-(I+DH)^{-1} g(\sigma, \phi_0) = y_0 \quad (4.4)$$

shows that  $y_0$  becomes unbounded as an eigenvalue of  $DH$  approaches  $-1$ . Chapter 5 shows four TCR circuit examples in which  $DH$  has eigenvalue approaching  $-1$  for different values of  $\sigma$ .

## 4.2 Switching time Bifurcations

When the harmonic components of the TCR current and voltage become very large, the current and voltage waveforms become highly distorted. These distortions can lead to instabilities as switching times suddenly change or bifurcate as follows:

*Instability when a new TCR current zero appears*

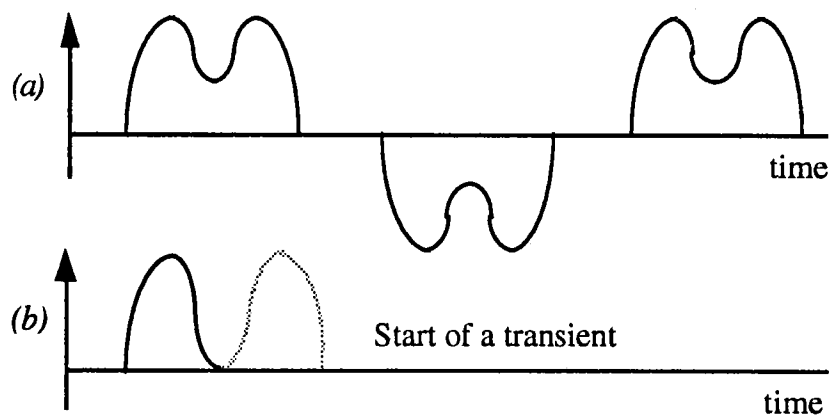


Figure 4.1. A new earlier TCR current zero appears  
 (a)  $\phi < \phi^*$ , (b)  $\phi = \phi^*$

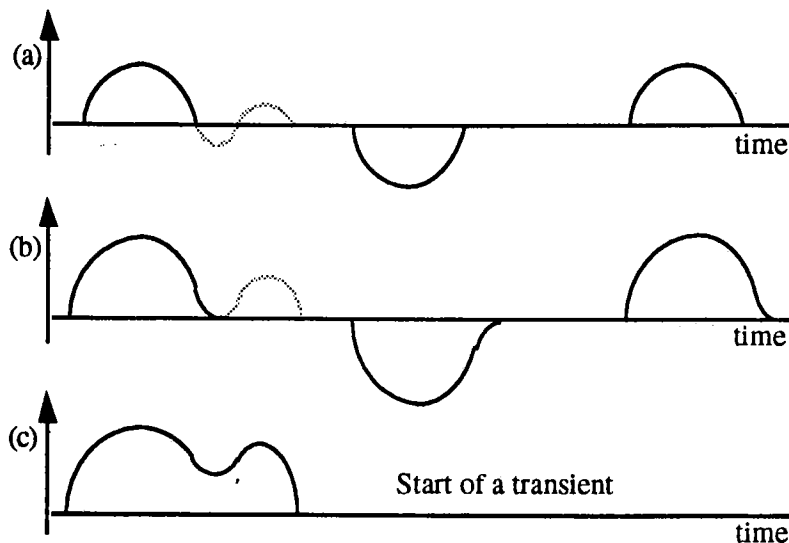


Figure 4.2. Disappearance of two TCR current zeros  
 (a)  $\phi < \phi^*$ , (b)  $\phi = \phi^*$ , (c)  $\phi > \phi^*$

### *Instability due to a thyristor misfire*

Figure 4.3 explains the onset of instability due to a thyristor misfire [26,38]. The TCR current is denoted with the solid line in the Figure 4.3a and starts conducting, as expected, when a firing pulse is applied. The gray lines in Figure 4.3 are used to show the thyristor current that would have obtained if we would have integrated the system backwards in time with the thyristor on and with the initial TCR current of zero at the firing time. As the firing pulses are moved towards the zero crossings of the TCR voltage, the TCR voltage blocked by the thyristors at the firing time decreases. Assuming thyristors are ideal, the critical phase  $\phi^*$  occurs when the turn on firing pulse is sent at the zero crossings of the TCR voltage as shown in the Figure 4.3b. As the phase  $\phi$  slightly increases from  $\phi^*$ , one of the thyristors misfires as the voltage across it is negative when the firing pulse arrives. In practice, the

map crosses the unit circle. (We assume that the system is initially operating in a stable periodic fashion before the bifurcation occurs.) The stable periodic orbit can disappear (saddle-node bifurcation) by coalescing with an unstable periodic orbit as an eigenvalue crosses the unit circle at 1. The stable periodic orbit can become modulated with another frequency or become unstable (Niemark or secondary Hopf bifurcation) as a complex conjugate pair of eigenvalues crosses the unit circle. Finally, the stable periodic orbit can double in period as an eigenvalue crosses the unit circle at -1 [46].

The importance of bifurcation theory as applied to the nonlinear circuits of power electronics is that it provides a short list of well known, typical ways in which the circuit can go unstable and some associated computational techniques to guide investigations. Several authors (e.g. [12,36,45]) have investigated instabilities such as Hopf and period doubling bifurcations in averaged models of fast switching power electronic circuits. One of the difficulties in applying bifurcation theory to the naturally commutated circuits which switch at a lower frequency lies in analytically or numerically computing the Jacobian of the Poincare map. One of the contributions of this thesis is to solve this problem for various circuit models.

## 4.4 Instabilities

We expect that switching time and conventional bifurcations as discussed in the sections 4.2 and 4.3 describe typical ways in which a TCR circuits become unstable. The following shows how conventional bifurcations

### *The constant sigma controller*

In all the firing schemes except the equidistant firing, the thyristor turn on time depend on the system state. For example, the constant sigma controller computes the thyristor turn on time based on the previous turn on and turn off times. In the constant sigma controller case, correction terms should be added to the Jacobian matrix  $J_{\text{equidistant}}$  given by (1), to obtain the Jacobian matrix  $J_{\text{sigma}}$  (for details refer to section 3.4.) In particular,  $J_{\text{sigma}}$  for the periodic solutions which are halfwave symmetric is given by:

$$J_{\text{sigma}} = (J_{\text{equidistant}} + \frac{c\dot{x}(\phi)}{2c\dot{x}(\phi + \sigma -)} c^t c e^{A\sigma} + \frac{c^t c}{2})^2 \quad (4.6)$$

In this formula,  $A$  is the linear system matrix when the thyristor is on,  $\sigma$  is the conduction time of thyristors and  $P$  is a non square constant projection matrix. The vector constant vector  $c$  is chosen such that  $c x(t)$  represents the TCR current at time  $t$ .  $c\dot{x}(\phi +)$  and  $c\dot{x}(\phi + \sigma -)$  denote the gradient of the TCR current as it turns on at time  $\phi$  and turns off at time  $\phi + \sigma$ . It is clear from the Figure 4.2b that as a thyristor turn off time disappears, the gradient of the TCR current as it turns off approaches zero and  $1/c\dot{x}(\phi + \sigma -)$  in (4.6) approaches infinity. Indeed, some of the eigenvalues of  $J_{\text{sigma}}$  for the circuit examples in chapter 5 cross the unit circle just before instability due to the disappearance of a thyristor current zero.

## Chapter 5

### Four TCR Circuit Examples Illustrating Bifurcation Instabilities

The classical analysis is often applicable, but can as described in chapter 4, fail for certain circuit parameters and operating conditions. Under these conditions, both the voltage and the current waveforms become greatly distorted with large harmonic components. The large harmonic distortions can lead to either switching time bifurcations or conventional bifurcations. This chapter gives four examples of such instabilities. The first example illustrates switching time bifurcation by the simulation of a SVC with realistic parameters. Simulation is used to show how the distortion of current waveforms can cause a thyristor turn off time to disappear or a new thyristor turn off time to suddenly appear. The second example shows switching time bifurcation in the Rimouski SVC using a hardware model.

During the early design phase of 230KV, 330 Mvar Advanced Series Compensator (ASC) system in northeastern Arizona at Kayenta an unexpected "second resonance" was observed [9]. Section 5.3 studies this example when the firing pulses are sent based on the constant sigma controller. In this case, the eigenvalues of the Jacobian matrix detect a conventional bifurcation just before a thyristor turn off time disappears. Upon loss of stability, the system converges to a nearby periodic solution which is no longer halfwave symmetric. The initial design was modified by doubling the size of the thyristor control reactor to remove this

### *Analysis*

In this example, the natural frequencies of the circuit from when the reactor is fully on to when it is fully off span the fifth harmonic. This crossing of an odd harmonic is an indication that the overall system odd harmonics can be large and that the voltage and current wave forms can be significantly distorted.

The half cycle Jacobian matrix has an eigenvalue at  $-0.97$  when the TCR conduction time  $\sigma \approx 50^\circ$ . This is the resonance condition discussed in the chapter 4. Figure 5.2 shows the TCR current sampled at the center of the conduction time versus  $\sigma$ . This Figure illustrate resonance at  $\sigma \approx 50^\circ$ .

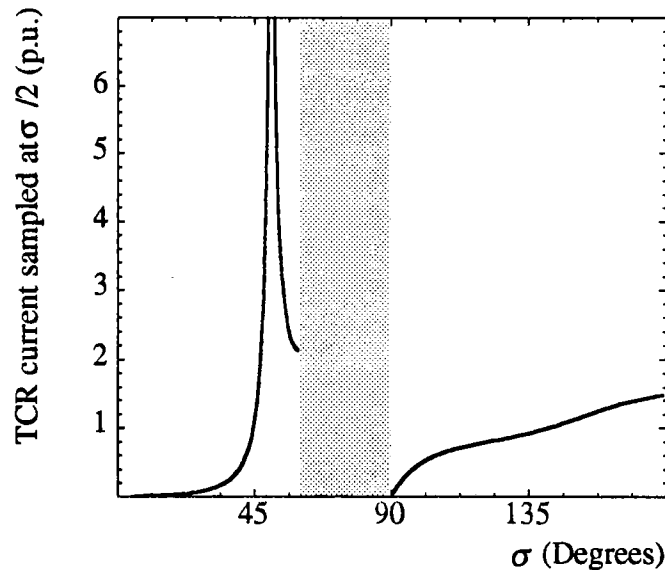


*Figure 5.2. TCR current sampled at  $\sigma/2$  versus  $\sigma$*

Figure 5.3 shows  $\sigma$  versus the firing phase  $\phi$ . Only periodic orbits which are half wave symmetric are computed. Figure 5.3 may be

### *Simulation Results*

The periodic orbits labelled 1 through 6 in the Figure 5.2 are chosen so as to study in detail how the harmonic distortion can cause periodic solutions to disappear in switching time bifurcations as the phase delay varies. The loss of a stable periodic solution at  $\sigma \approx 91^\circ$  is a switching time bifurcation in which a new TCR current zero appears. The simulation in Figures 5.4 show periodic solutions of the TCR current at periodic orbits 1, 2 and 3 respectively. Note that as we move towards the third periodic orbit, the harmonic distortion produces a dip in the TCR current. Figure 5.3c shows that as the phase delay of the firing pulses is slightly increased so as to pass the third periodic orbit, the dip in the TCR current lowers and a new, earlier zero of the TCR current is produced. The switch off time of the thyristor has suddenly decreased and the stable operation of the system at the previous periodic orbit has been lost in a switching time bifurcation and a transient starts.

Even though many systems enforce equidistant firing in steady state operation, the firing pulses may or may not be equidistant during transients. Therefore, the detail of the transient depends heavily on the assumptions used in modelling the control of the TCR firing pulses. The intent of time domain simulation is to show the existence of the transient as a consequence of the switching time bifurcation rather than the detail of the transient. However, computations of steady state periodic orbits as in Figure 5.3 are valid for any firing control scheme that enforces equidistant firings in steady state.



The loss of a stable periodic solution at  $\sigma \approx 56^\circ$  is a switching time bifurcation in which a TCR current zero disappears. Figure 5.5 shows how the periodic solutions behave as the switching time bifurcation is approached. The plots are on an expanded time scale so as to closely observe the zero current turn off behavior of the thyristors. The dotted lines show the current in thyristors that would have occurred if the thyristors did not turn off as the current decreased through zero. This part of the current is referred to as the virtual part of the current. The virtual current does not occur in the circuit operation but it is important in understanding how the TCR current zero disappears.

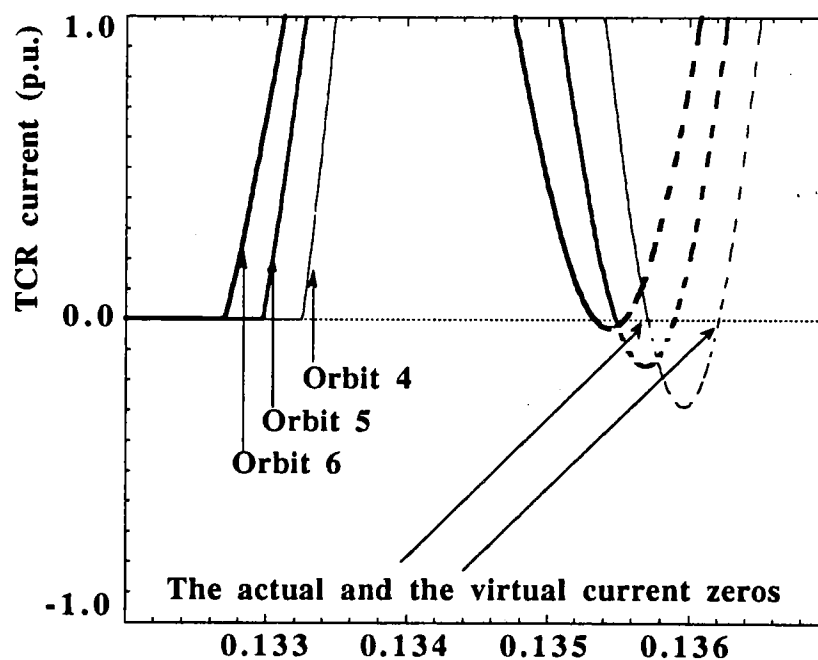


Figure 5.5. Periodic orbits 4,5 and 6

## 5.2 The Rimouski static VAR compensator

The static VAR compensator installed near Rimouski, Quebec is shown in the Figure 5.7 [35]. This compensator is a three phase delta connected TCR and ungrounded wye-connected capacitor banks interfaced to a 230 kV system through a step down transformer.

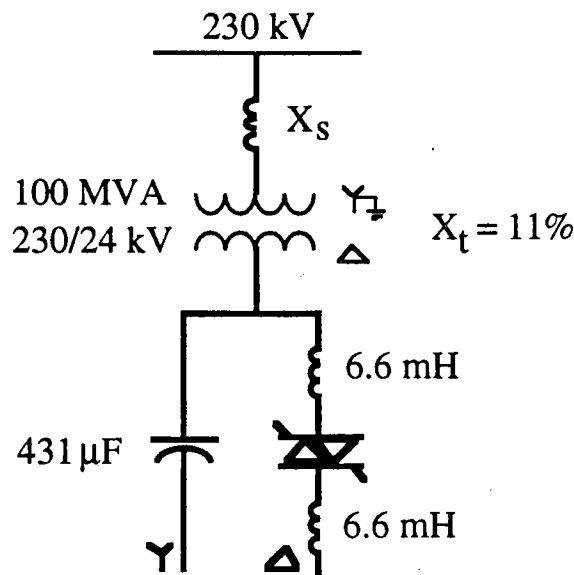


Figure 5.7. Rimouski static VAR compensator

### *Experimental setup*

An experiment was used to confirm the theoretical computations. This setup used a 115 V, 60 Hz AC line which was assumed to be a stiff and harmonic free source. The circuit components were scaled as shown in Table 5.1. The reactance to resistance ratio was measured as approximately 20 for the inductors and approximately 70 for the capacitor. The control circuit used a zero voltage detector synchronized directly across the AC line and a firing pulse generator to build a train of

system converges to a new steady state at the point B+. This instability occurs when the thyristor turn off time is suddenly increased due to the disappearance of the thyristor current zero.

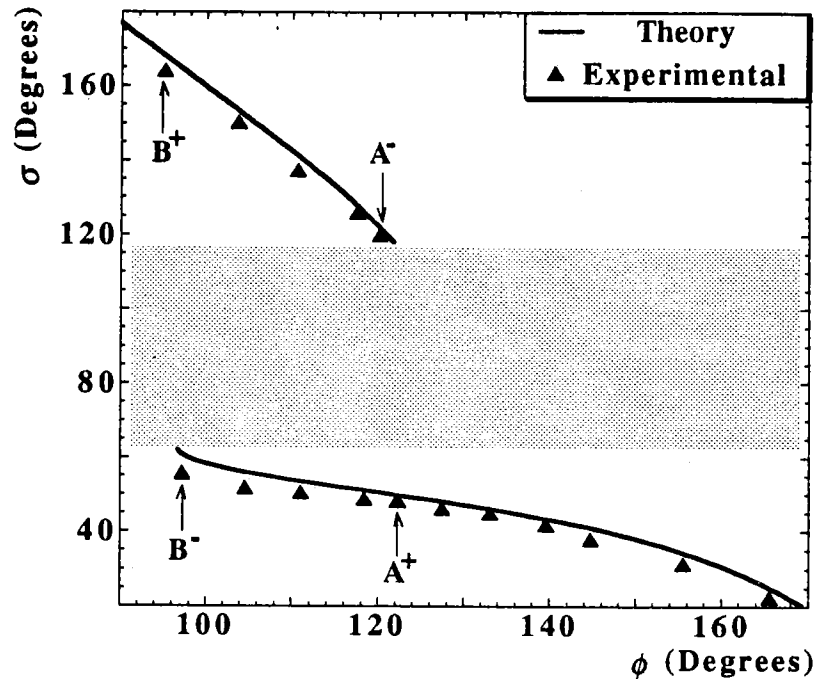


Figure 5.8.  $\phi$  versus  $\sigma$

The bifurcation instabilities are associated with the two natural frequencies of the circuit (the TCR fully on and fully off) spanning the 3rd harmonic number. For example, when the short circuit MVA of the system is infinite ( $X_s = 0$ ), the two natural frequencies do not span the 3rd harmonic and the bifurcation instabilities are absent. The half cycle Jacobian matrix has an eigenvalue at -1 for the circuit operating at the conduction time  $\sigma \approx 40^\circ$  (ignoring the circuit resistances.) This is the resonance condition discussed in the chapter 4.

### Analysis

Figure 5.10 shows the predicted resonance points using the average inductor model (chapter 3.2) as  $\sigma$  varies from zero to  $180^\circ$  for three possible values of  $L_r$ , namely 1.7 mH, 3.4 mH (initial design) and 6.8 mH (final design). This model predicts potential problems at the 3rd harmonic resonance point for  $\sigma \approx 158^\circ$  when  $L_r = 3.4$  mH.

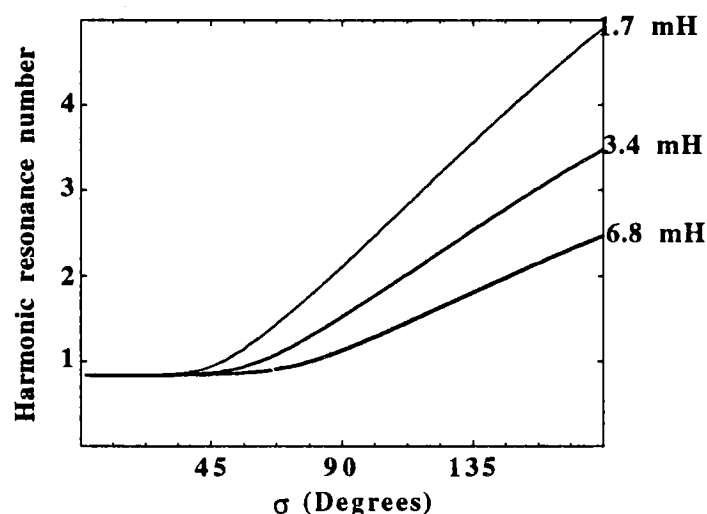


Figure 5.10. Resonance predictions using the average inductor model

The half cycle Jacobian has an eigenvalue close to -1 for the circuit operating at the conduction times  $\sigma = 49.5^\circ$  and  $\sigma = 156.9^\circ$ . These two points correspond to the expected fundamental resonance and the unexpected "second resonance" observed in [8]. The fundamental and the 3rd component of the TCR current versus the control parameter  $\sigma_p$  are shown in the Figure 5.11. The solid lines denote the periodic solutions which are halfwave symmetric. The circles denote the periodic solutions which are T periodic but not halfwave symmetric.

attempts to find another nearby periodic solution but is not successful.

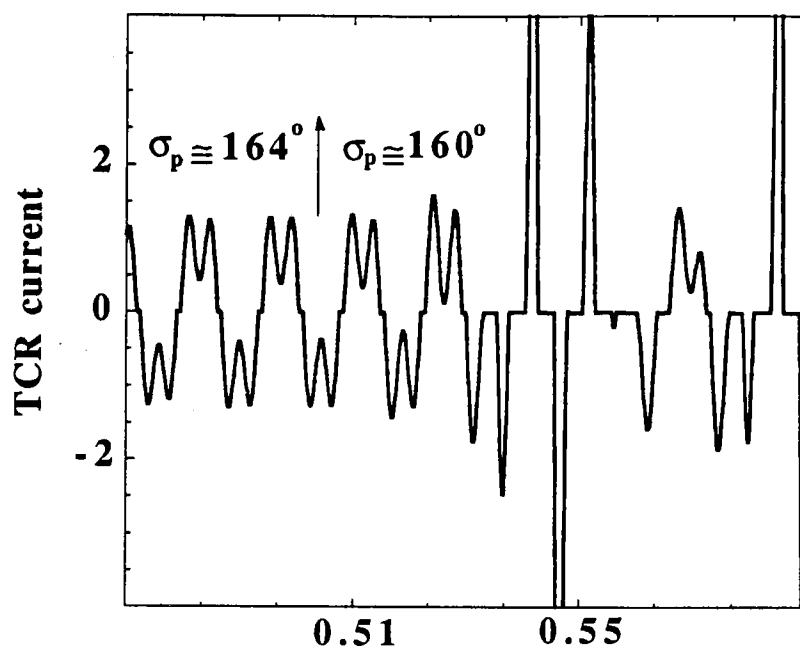


Figure 5.12.  $\sigma_p$  steps down from  $164^\circ$  to  $160^\circ$

Figure 5.13 shows the transient which occurs as  $\sigma_p$  steps up from  $115^\circ$  to  $120^\circ$ . A transient starts when the TCR current misses the first current zero and the system converges to another periodic solution which is no longer half wave symmetric.

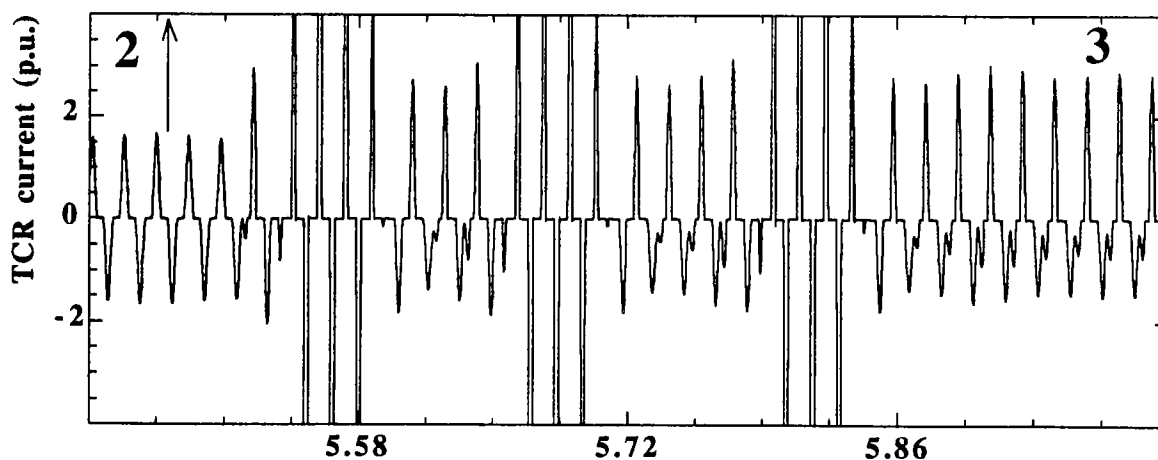


Figure 5.13.  $\sigma_p$  steps up from  $115^\circ$  to  $120^\circ$

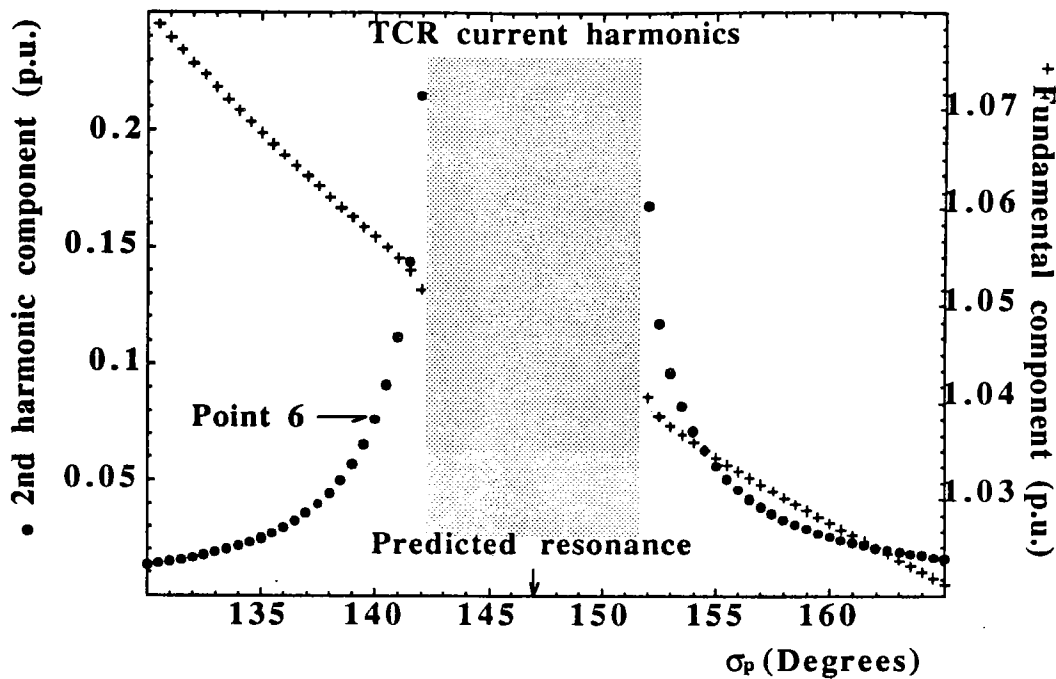


Figure 5.14. The fundamental and the 2nd component of the TCR current

### Simulation results

The transients as  $\sigma_p$  steps up from  $140^\circ$  to  $144^\circ$  is studied. The system is initially in steady state as shown in the Figure 5.15. Figure 5.16 shows the transient in the TCR current as  $\sigma_p$  is increased by  $4^\circ$ . Figure 5.16 shows the ASC voltage across the TCR and the firing pulses sent to the back to back thyristors. As the system drifts towards the new steady state solution, the ambient 2nd harmonic voltage across the TCR magnifies. This produces an increasing asymmetry in the ASC voltage waveforms which eventually results in a thyristor misfire and thus the loss of previous periodic solution.

## 5.5 Summary

This chapter studied examples of resonance, harmonic distortions and bifurcations using four different TCR circuits. Switching time bifurcation instabilities in which switching times suddenly change and the system stability is lost were illustrated by both simulation and experiment. The first two sections studied a static VAR compensator with realistic system parameters. The last two sections focused on the initial and the final design of the advanced series compensator installed near the Kayenta substation. It was shown how the initial design suffered from large harmonic distortions in the TCR current and bifurcation instabilities. In addition, it was shown that the final design contains a resonance point which can lead to the bifurcation of the periodic solutions when stimulated with ambient even harmonics.

## Chapter 6

### Nonlinear Dynamics and Damping

The dynamics of a Thyristor Controlled Reactor (TCR) circuit are nonlinear since the thyristor turn off time depends on the system state via the TCR current. The thyristor turn on time may also depend on the system state via the firing scheme. The nonlinear dynamics of a TCR circuit can be studied by means of a Poincare map which advances the system state by one period of the fundamental frequency. When the circuit is in steady state, the Poincare map has a corresponding fixed point. When the TCR circuit is transient (diverging away or converging towards a periodic trajectory), the Poincare map also has a corresponding transient (diverging away or converging towards a fixed point.)

Chapter 3 derived the Jacobian of the Poincare map for four different firing schemes. The Jacobian evaluated at the fixed point approximates the nonlinear dynamics of the Poincare map close to the fixed point by a discrete time linear map.

One of the useful contributions of this thesis is to use the Jacobian to illustrate the concept of attenuation or damping. Damping exists even when the circuit resistances are ignored and the thyristors are assumed ideal (short circuit when they are conducting, and open circuit when off). Presently, one of the most common techniques for the study of damping is to compute the eigenvalues of the system by replacing the TCR with a



Write  $F$  for the Poincare map which advances the state by one period of the fundamental frequency  $T$ .  $F$  can be computed by integrating the system equations and taking into account the switching between the on and off systems. In particular we choose  $F$  to advance the state  $y(\phi_0)$  at turn on to the state  $y(\phi_0+T)$  one period later. Assume that the circuit is in steady state and the firing pulses are delayed by  $\phi_0$ . If the periodic orbit passes through  $y_0$  at time  $\phi_0$ , then  $y_0$  is a fixed point of the map  $F$  and  $F(y_0)=y_0$ .

To illustrate the concept of damping, add a small perturbation of  $\epsilon_0$  to  $y_0$  just before the thyristor firing pulse arrives at time  $\phi_0$ . The circuit propagates  $\epsilon_0$  as time passes. The map  $F$  can be used to compute  $\epsilon_1$ , the deviation from  $y_0$  one period later as follows:

$$\epsilon_1 = F(y_0+\epsilon_0)-y_0$$

$F(y_0+\epsilon_0)$  can be expanded about  $y_0$  as:

$$\epsilon_1 = DF \epsilon_0 + \text{higher order terms}$$

Hence, the eigenvalues of  $DF$  can be used to check if  $\epsilon_0$  damps or not. For example, when the eigenvalues are inside the unit circle, the periodic orbit is asymptotically stable and the system damps out small perturbations. Assuming half wave symmetry for the periodic solutions,  $DF$  is (see chapter 4.3)

$$DF = (e^{PAP^t(T/2-\sigma)}Pe^{A\sigma P^t})^2 \quad (6.1)$$

Much insight into the properties of the Jacobian formula can be obtained

resistance in the circuit.) At the switch off time,  $E_0$  decreases by the energy stored in the reactor  $L_r$  at time  $\phi_0 + \sigma$  which is a nonnegative quantity. Since  $E_k$  is a Liapunov function for the discrete time system  $\delta_{k+1} = DF \delta_k$ ,  $k=0,1,2,\dots$ ,  $DF$  must be stable. If the circuit resistance are included, then  $E_k$  is strictly decreasing when the switch is on or off and  $E_k$  is strictly Liapunov function and  $DF$  is asymptotically stable.

It is the switch off which projects the TCR current to zero at time  $\sigma$  and damps the perturbations. Although the circuit model for the Jacobian is very useful in understanding the nature of  $DF$ , we caution that the sudden loss of energy at the switch off for the Jacobian model is nonphysical and does not describe the gradual damping of a perturbation by dissipation in the source of the SVC circuit.

## 6.2 Numerical examples

The following are three examples illustrating the nonlinear dynamics and damping in TCR circuits.

### *Example 1*

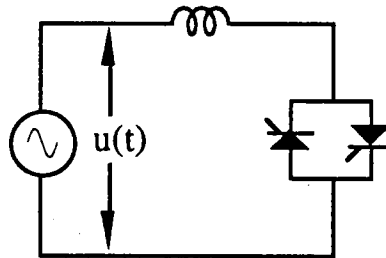


*Figure 6.3. The simplest TCR circuit which illustrates damping ( $R=0$ )*

Figure 6.3 is the simplest TCR circuit which illustrates damping when the

Figure 6.5a shows the eigenvalues of DF in (6.1) inside the unit circle as  $\sigma$  ranges from  $0^\circ$  to  $59^\circ$  and from  $90^\circ$  to  $180^\circ$ . For  $\sigma$  between  $59^\circ$  and  $90^\circ$ , stability is lost due to a switching time bifurcation (chapters 4.2 or 5.1). Figure 6.5b shows the eigenvalues when the circuit resistances are ignored.

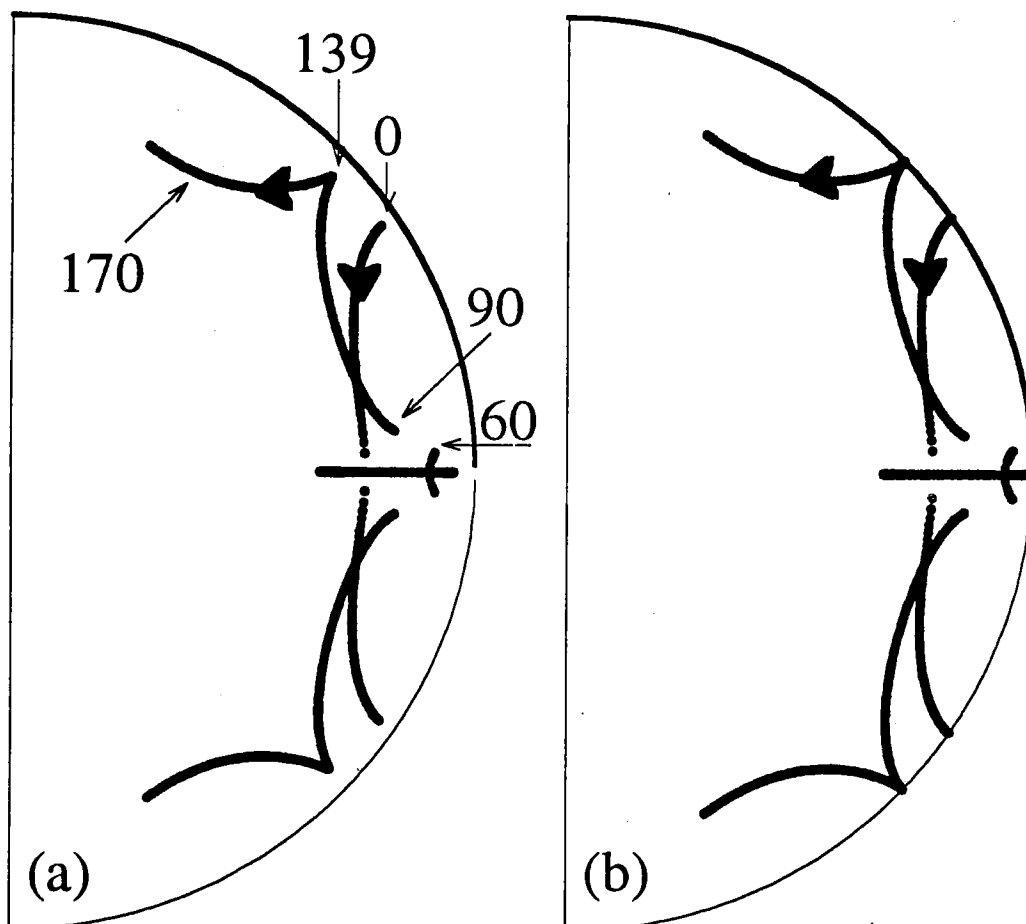


*Figure 6.5 The eigenvalues of DF ( $0^\circ < \sigma < 59^\circ$  &  $90^\circ < \sigma < 180^\circ$ )  
 (a) circuit resistance included (b) circuit resistances set to zero*

The circuit model developed for the Jacobian (see Figure 6.2) can be used to explain and predict  $\sigma \approx 139^\circ$ , the  $\sigma$  at which the eigenvalues touch the unit circle (case with no resistances). The energy associated with

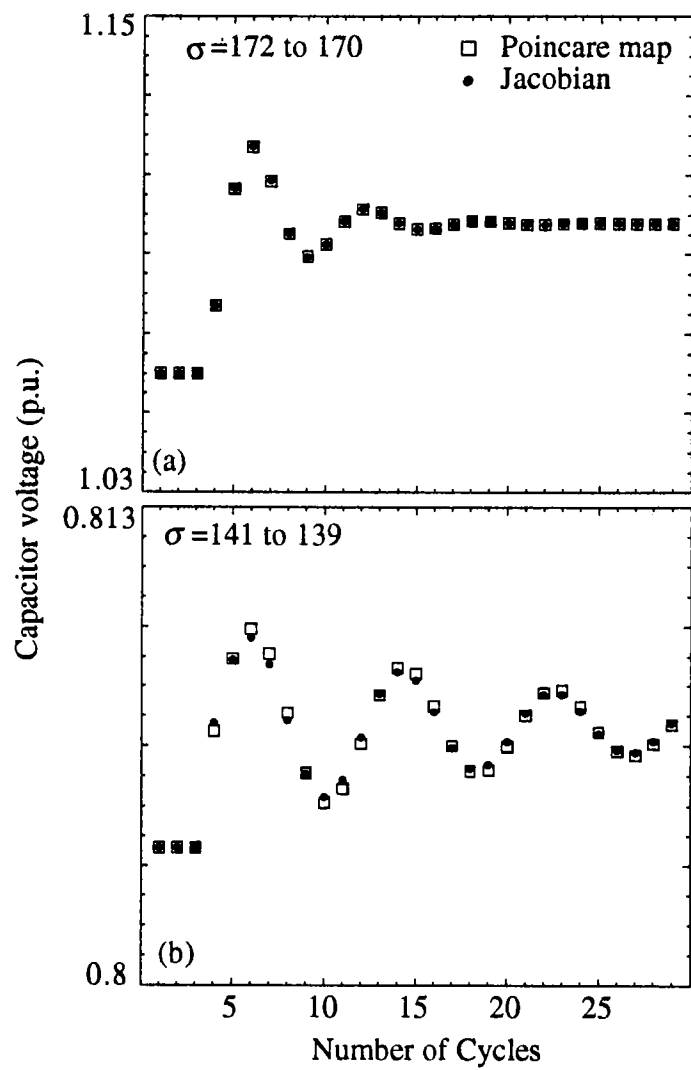


Figure 6.6 Dynamic response as  $\phi$  is changed  
 (a)  $\sigma = 172^\circ$  to  $170^\circ$  (b)  $\sigma = 141^\circ$  to  $139^\circ$

### Example 3

The circuit diagram shown in Figure 6.8 is the Advanced Series compensator(ASC) installed near the Kayenta substation. The system parameters are  $L_s'+L_s''=405.8$  mH,  $R_s=19.89$   $\Omega$ ,  $C_r=177$   $\mu$ F,  $C_s=27.9$   $\mu$ F and  $L_r=6.8$  mH.

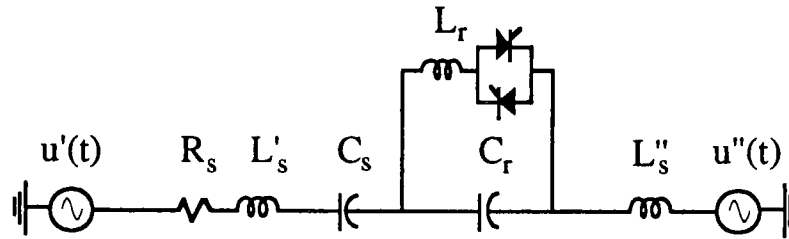


Figure 6.8. The ASC installed near Kayenta

The research group at Siemens use the EMTP to study the open loop response of Kayenta system to  $4^\circ$  step changes in the TCR conduction time  $\sigma$  when the firing is synchronized on the zeros of the voltage [17]. This study is reproduced in the Figure 6.9 for  $\sigma=40^\circ$ ,  $50^\circ$  and  $60^\circ$ .

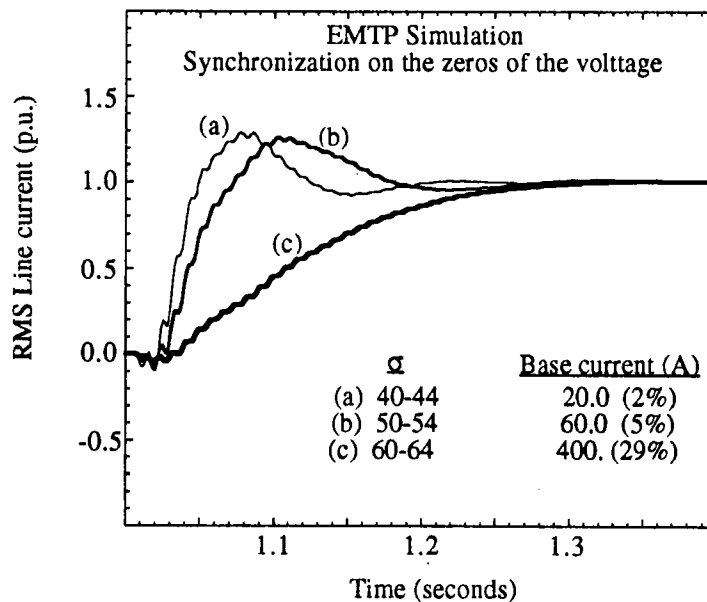


Figure 6.9. ASC response to  $2^\circ$  step change in  $\alpha_v$  (from EMTP)

large perturbation as compared to 2% and 5% for the cases (a) and (b). Hence, discrepancy between the Jacobian predictions and the actual Poincare map simulation for the case (c) is not unexpected. We can immediately observe from Figures 6.9 and 6.10 that the firing scheme and the operating point of the TCR has a significant impact on the dynamic response of the Kayenta advanced series compensator.

### 6.3 Summary

The dynamic response of a TCR circuit is nonlinear and can be studied using the Poincare map. The Poincare map of a TCR circuit is a smooth and differentiable function of the system state except at switching time bifurcations. This map advances the system state by one period of the fundamental frequency. If the system state is a periodic trajectory, then the state is a fixed point of the map. The Jacobian of the map evaluated at the fixed point can be used to approximate the nonlinear dynamics of the Poincare map close to the fixed point by a discrete time linear map.

The eigenvalues of the Jacobian were used to show that a TCR circuit can damp small perturbations even when the circuit resistances are ignored and the thyristors of the TCR are assumed ideal. This concept of damping can not be explained by the classical method which models the TCR with an variable linear inductor. Three numerical examples were used to illustrate the concept. In particular, it was shown that the dynamic response of TCR circuit can heavily depend on the TCR firing scheme and conduction time.

# Chapter 7

## Single Phase Thyristor Bridge

This chapter extends some of the tools and the thinking developed for the single phase TCR to a single phase line commutated bridge. To illustrate some of the potential problems and the tools developed in this chapter, we will use the system in Figure 7.1.

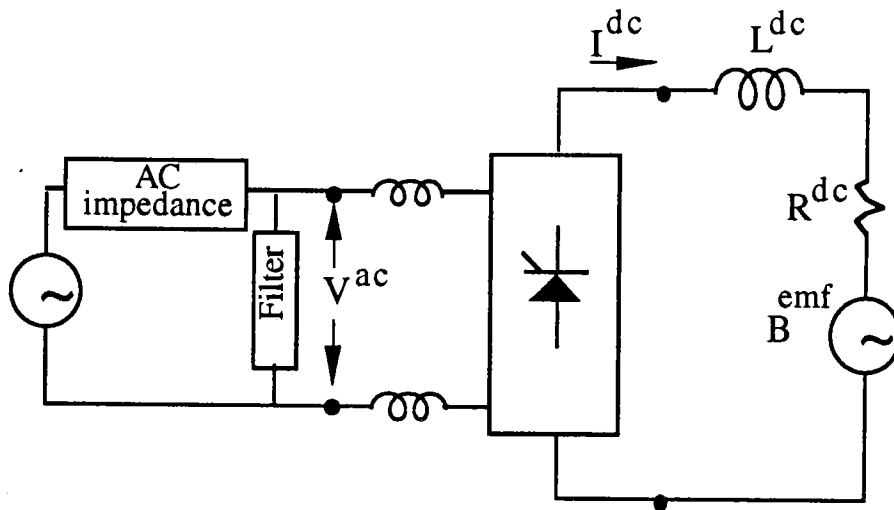


*Figure 7.1. Basic System*

This circuit has a thyristor bridge with a dc load in series with a dc source. The ac system is a general linear, frequency dependent impedance with ac filters located at the terminals of the converter. The thyristors are assumed ideal so that nonlinearities in the turn on/off of the thyristors are neglected.

Solving the equations (7.1) and (7.2) for  $V_{dc_{n=0}}$  and  $\mu$  allows us to construct the steady state waveforms of the inverter AC current and DC voltage at a given operating point. For this operating point, the inverter AC current harmonics,  $I_{ac_n}$  and DC voltage harmonics,  $V_{dc_n}$  can now be calculated by doing a Fourier analysis on the corresponding inverter steady state waveforms.

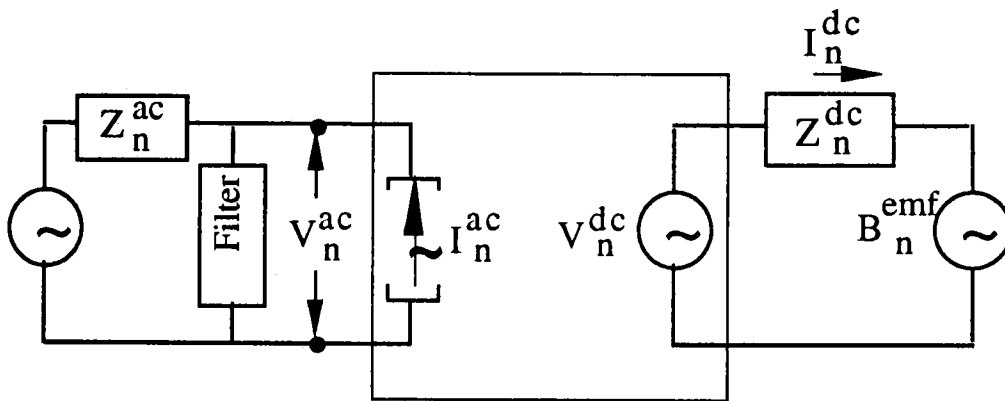


Figure 7.2. Classical model for calculating the  $I_{dc_n}$  and  $V_{ac_n}$

To calculate  $I_{dc_n}$  and  $V_{ac_n}$ , the converter is replaced by an equivalent AC harmonic current source,  $I_{ac_n}$  and an equivalent DC harmonic voltage source,  $V_{dc_n}$  as shown in Figure 7.2. Section 7.3 provides an example in which the classical solution method is not correct.

## 7.2 Harmonic Coupling Matrix Solution Method

This section develops a harmonic coupling matrix for the single phase convertor shown in the Figure 7.3. This matrix shows the coupling between the convertor harmonics which is an important characteristics of all naturally commutated thyristor switching circuits. Moreover, we will show how this matrix can be incorporated into a power system network



equivalents as seen from the converter terminals allows us to write the following general equation for  $V^{ac}$  and  $I^{dc}$ .

$$\begin{bmatrix} F^{ac} \\ B^{emf} \end{bmatrix} = \begin{bmatrix} I + Z^{ac}A & Z^{ac}B \\ C & D - Z^{dc} \end{bmatrix} \begin{bmatrix} V^{ac} \\ I^{dc} \end{bmatrix} \quad (7.4)$$

where the matrices  $Z^{ac}$  and  $Z^{dc}$  are diagonal and of infinite dimensions denoting the Thevenin AC and DC impedances.  $I$  is the identity matrix and  $F^{ac}$  and  $B^{emf}$  are vectors of infinite dimension representing the Thevenin AC and DC sources.

In appendix A, we use the switching function technique to derive the  $A, \dots, D$  matrices. The basic idea was first introduced in [21] for switching circuits with fixed switching times. In [7], Bohmann and Lasseter extend this method to circuits which include one naturally commutated switching elements. The switching functions used to derive the harmonic coupling matrix are shown in the Figure 7.4. In this Figure, the switching functions  $H^1(\omega t)$  and  $H^3(\omega t)$  carry the on/off information of the thyristor pairs  $(S_1, S_2)$  and  $(S_3, S_4)$  respectively. For example,  $H^1(\omega t)$  has a value of one when the thyristor pair  $(S_1, S_2)$  is conducting and zero when they are off.

The two switching functions  $H^{13}(\omega t)$  and  $H^{31}(\omega t)$  uniquely define the commutation process from one thyristor pair to another. For example, the application of a firing pulse at time  $\phi_1$  to the thyristor pair  $(S_1, S_2)$  starts a commutation process from the switches  $(S_3, S_4)$  to  $(S_1, S_2)$ . This commutation process is defined by the switching function  $H^{31}(\omega t)$  with a

$$I^{ac}(\phi_2 + \mu_2) = -I^{dc}(\phi_2 + \mu_2) \quad (7.6)$$

We refer to the equations (7.5) and (7.6) as constraint equations since they constrain the commutation times  $\mu_1$  and  $\mu_2$ . Using the formalism developed in the appendix A, the constraint equations can be written in terms of the Fourier components of the converter AC voltage and DC current as follows:

$$\sum_{\substack{m=-\infty \\ m \neq 0}}^{\infty} \frac{V_m^{ac}}{jm\omega L} e^{jm\phi_1} [e^{jm\mu_1} - 1] = \sum_{m=-\infty}^{\infty} I_m^{dc} e^{jm\phi_1} [e^{jm\mu_1} + 1] \quad (7.7)$$

$$\sum_{\substack{m=-\infty \\ m \neq 0}}^{\infty} \frac{V_m^{ac}}{jm\omega L} e^{jm\phi_2} [e^{jm\mu_2} - 1] = - \sum_{m=-\infty}^{\infty} I_m^{dc} e^{jm\phi_2} [e^{jm\mu_2} + 1] \quad (7.8)$$

where  $V_m^{ac}$  denotes the  $m$ th harmonic component of the AC bus voltage,  $\omega$  is the operating frequency and  $L$  is the commutating inductance. Equations (7.3), (7.4) are infinite matrices and the constraint equations (7.7) and (7.8) are infinite sums. Assuming that the higher harmonics can be neglected, these infinite matrices and sums can be approximated with finite matrices and sums by truncating them at a reasonably high harmonic. Trial and error has shown that truncating above the 20th harmonic is reasonable.

The solution algorithms of the harmonic coupling equations are slightly different for different control schemes. This is because each control scheme impose a different constraint on the thyristor firing angles,  $\phi_1$

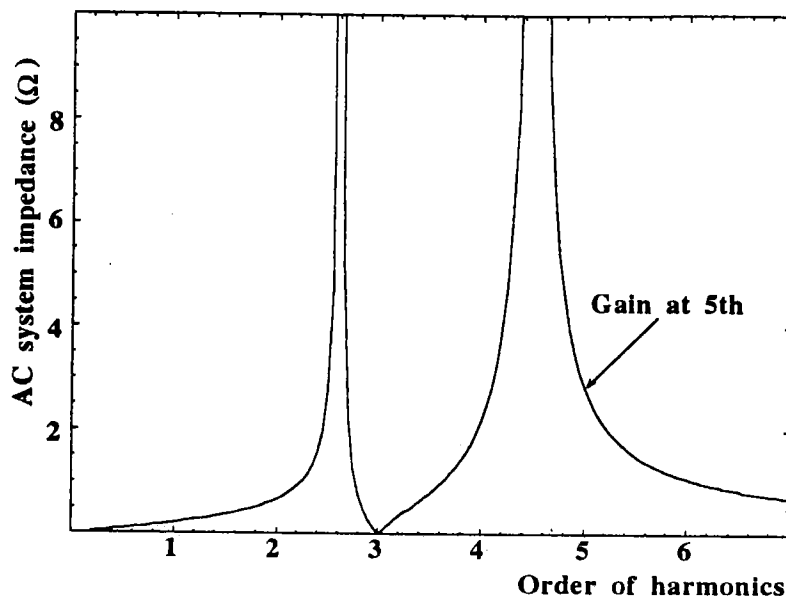


*Figure 7.5 The impedance of the AC system*

This example has a short circuit ratio of 5.0 where this ratio is defined as the AC short circuit MVA divided by the rated DC power. A short circuit ratio of 5.0 was used to demonstrate the nonlinear harmonic interaction problems with a high impedance AC voltage source. Trial and error has shown that even a very strong AC system will show such problems if the AC systems resonance point is close enough to an odd harmonic number. For example, an AC system with a short circuit ratio of 25.0 shows harmonic resonance problems when the resonant point is 4.85 times the fundamental frequency.

### *Periodic solutions and stability*

An equidistant firing pulse scheme in which a train of equally spaced firing pulses  $180^\circ$  are sent to convertor is assumed. For each phase of the firing pulses, the circuit is solved using both the classical and the

(7.2). The point  $I_{dc} \approx 0$  corresponds to the largest phase of the firing pulses,  $\alpha_{max} = 60^\circ$ . At this point, the average inverter DC voltage is equal to the DC side  $B^{emf}$ . As  $\alpha$  is decreased, the average inverter DC voltage and the DC current increase. The larger the DC current, the longer it takes to commute the current from one thyristor pair to another, and the larger the  $\mu$ . The maximum values of the DC current and  $\mu$ , correspond to  $\alpha_{min} \approx 20^\circ$  and  $\mu \approx 58^\circ$ .

While the classical method predicts a smooth mapping between the DC current and  $\mu$ , the harmonic coupling method predicts a discontinuous map made up of three separate regions. These three regions are labelled region A, region B and the shaded region.

In the region A, the DC current decreases as  $\mu$  decreases. This region exists for  $\mu$  ranging between  $49^\circ$  and  $58^\circ$ . The consequence of moving the system operating point from region A into the shaded region is a transient due to the appearance of a new earlier current zero in the commutating thyristor pair. This new earlier zero results in the switching off time of the thyristor to be suddenly decreased and the stable operation of the system at the previous periodic orbit to be lost. The loss of a stable periodic solution is due to a switching time bifurcation in which the thyristor turn off time is suddenly decreased. For an equidistant firing, the absolute value of all of the eigenvalues of the Jacobian are less than 1 as the system moves towards the shaded region [13]. This implies that no conventional bifurcation precedes the switching time bifurcation.

that the measured value of  $\mu$  at C- is the predicted value of  $\mu$  as the boundary of region A with the shaded region. Measurement of  $\mu$  at the boundary of (C- ,C+) show that the value of  $\mu$  has a step drop from  $49^\circ$  before C- to  $14^\circ$  after C+. After time C+, the value of  $\mu$  oscillates between  $14^\circ$  and  $7^\circ$  and gradually converges to  $10^\circ$ . This is the same value of  $\mu$  predicted by the harmonic coupling matrix solution method.

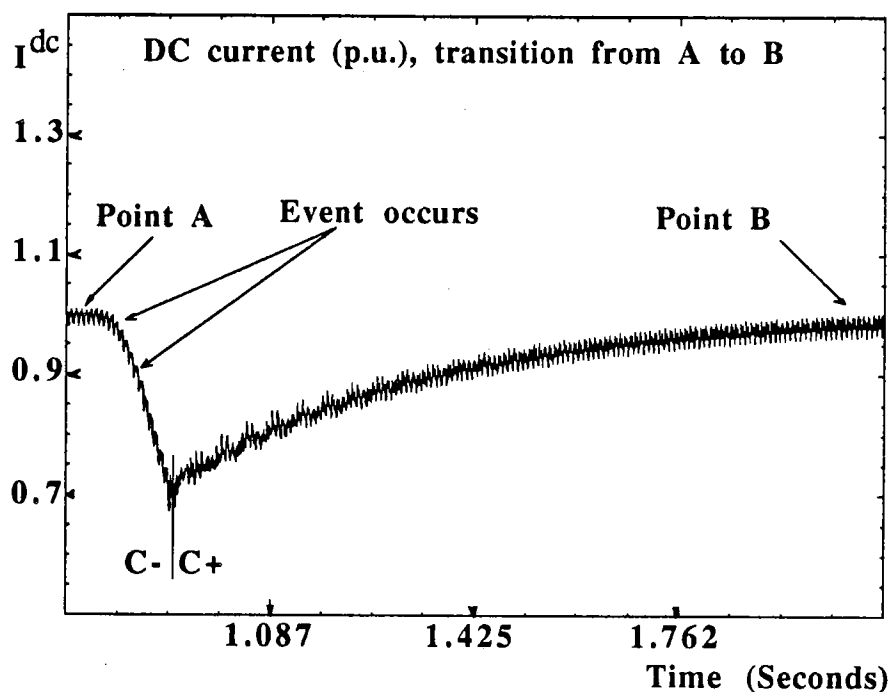


Figure 7.7. Inverter DC current ( from A to B)

To look at the commutation times more closely, only one cycle of the DC current in the Figure 7.7 is plotted in the next two Figures. The Figure 7.8 shows the steady state operation at the point A and the Figure 7.9 shows the steady state operation at the point B. It is clear from these Figures that the example system has two periodic solutions with DC currents close to 1.0 p.u. but two  $\mu$  and harmonic contents.

## 7.4 Summary

For the regions where periodic solutions exist, we can use Fourier techniques to accurately determine the harmonic contents of the steady state solutions. In this method, the voltage and switching functions are broken into Fourier series and a harmonic coupling matrix model of a single phase line commutated converter is constructed. This coupling matrix can be incorporated into a power system and the system harmonics can be accurately calculated. An example system which exhibits highly nonlinear and unexpected behavior was used to illustrate the effectiveness of this method. This example showed that classical solution method fails to correctly compute the harmonics of this example. On the other hand, the harmonic coupling matrix solution method can accurately compute the steady state solutions of this system.

Poincare map for different TCR firing schemes. The Jacobian formulas are used to show how the circuit dynamics depend on the TCR operating point and the TCR firing scheme. In particular, it is shown that a TCR circuit can damp small perturbations even when the circuit resistances are ignored and the thyristors are assumed ideal. This information about the circuit dynamics has not been explained or exploited by others.

2) Another contribution of this thesis is the concept of switching time bifurcations. It is shown that large distortions of the TCR current or voltage waveforms can lead to switching time bifurcations associated with either a new earlier TCR current zero, the disappearance of the TCR current zero, or a thyristor misfire. The switching time bifurcations are not explained by the classical analysis of TCR circuits, which assumes no distortion of voltage and current waveforms. Nor are the switching time bifurcations explained by the conventional theory of bifurcations in which stability is lost when eigenvalues of a Jacobian matrix cross the unit circle. However, it is possible to lose stability in a conventional bifurcation just before a thyristor turn off time disappears.

The following describes various aspects of these concepts in more detail.

### *Jacobian of the Poincare map*

Except for marginal cases, the Poincare map can be differentiated and a formula for its Jacobian can be obtained. Several authors have derived procedures for the Jacobian of various switching circuits [29,47,48]. A simple formula for the Jacobian when the firing pulses are equidistant is

the Kayenta substation. Using the Jacobian formulas and simulation, this thesis demonstrated that the TCR firing scheme and its operating point must be taken into account when studying the dynamics of the advanced series compensators (cf. chapter 6.2).

### ***Resonance***

Bohmann and Lasseter show that for certain circuit parameters and operating conditions the TCR current and voltage waveforms can become highly distorted. This thesis relates the large harmonic distortions to the circuit operating close to its resonance point. The circuit has resonance when one of the eigenvalues of a particular matrix is -1. This matrix is equal to the Jacobian of the half wave map of the circuit when the firing is equidistant.

### ***TCR circuit examples illustrating switching time bifurcations***

The EMTP simulation of a static VAR example with realistic circuit components were used to illustrate switching time bifurcations. In particular, it was shown how the distortion of the voltage and current waveforms could cause a thyristor switch off time to disappear or a new thyristor switch off time to suddenly appear. As a consequence of switching time bifurcations, the stable periodic operation of the circuit is lost and a transient starts. Switching time bifurcations were also illustrated using experiment for the single phase equivalent of the Rimouski static VAR compensator.



illustrate that the tools and the thinking developed for a TCR should be extended to naturally commutated converters.

## 8.2 Future work directions

Our main objective was to develop new ways of understanding and computing instabilities of general switching circuits. The following is a list of options for future work.

### *Generalizing the harmonic admittance methods*

The harmonic coupling matrix solution method has been a key tool in allowing us to quickly solve for the periodic solutions of the system. Therefore, it is reasonable to extend this method to arbitrary switching circuits. Combining a harmonic coupling matrix method with the existing power flow program will give a single useful and powerful program. This program could be used to study examples which contain more than just one converter connected to a power system network.

### *Better understanding of the conventional bifurcations*

This thesis showed that a circuit can lose stability in a conventional bifurcation when it is operating close to a switching time bifurcation, but how close is close? Using linear techniques and classical equations, Ainsworth showed that synchronizing the firing on the zeros of the voltage can introduce voltage instabilities. Is this voltage instability a conventional bifurcation which can be explained through the eigenvalues of Jacobian? What happens when the firing is synchronized on the TCR

this thesis does not take into account the detailed generator models. Since advanced series compensators are used to damp SSR, it is necessary to extend the Jacobian formulation to include generator models.

## Appendix A

### Harmonic Admittance of a TCR

The derivation of the harmonic admittance for the TCR is the same as [7] except for a slight modification. Consider the single phase TCR shown in Figure A.1. The thyristors are gated once each half cycle allowing control of the current in the reactor and thus allowing control of the reactive current drawn by the circuit.

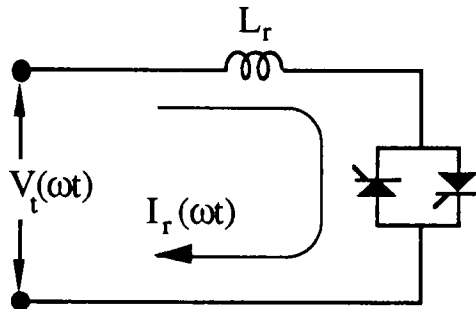


Figure A.1. Thyristor controlled reactor

The switching function,  $H(\omega t)$ , shown in Figure A.2 has a value of one whenever a thyristor is on and zero when the thyristors are off. Since a thyristor turns off when its current goes through zero, the conduction time  $\sigma$  depends on the turn on time  $\phi$ , the terminal voltage  $V_t(\omega t)$  and the TCR reactance,  $L_r$ . Therefore the switching function is dependent on the terminal voltage through the turn on/off time of the thyristors.

Equation (2) shows the time domain relationship among the terminal voltage, reactor current and the switching function. The constraint equations in (1) show how the switching function is dependent on the terminal voltage through the thyristor switching times  $\sigma$  and  $\phi$ .

Assuming periodicity,  $H(\omega t)$  can be represented by their complex Fourier series:

$$H(\omega t) = \sum_{n=-\infty}^{\infty} h_n(\sigma_1, \phi_1, \sigma_2, \phi_2) e^{jn\omega t} \quad (3)$$

where

$$h_0 = \frac{1}{2\pi} (\sigma_1 + \sigma_2) \quad (4)$$

$$h_n = \frac{j}{2n\pi} [e^{jn\phi_1}(e^{-jn\sigma_1} - 1) + e^{jn\phi_2}(e^{-jn\sigma_2} - 1)] \quad (5)$$

$\sigma_1 = \sigma_2$   
 $\phi_1 = \phi_2$

$$h_n = \frac{e^{jn\phi}(e^{-jn\sigma} - 1)}{-jn\pi}$$

Similarly, representing  $V_t(\omega t)$  and  $V_r(\omega t)$  by their complex Fourier series:

$$V_t(\omega t) = \sum_{m=-\infty}^{\infty} v_{tm} e^{jm\omega t} \quad (6)$$

$$V_r(\omega t) = \sum_{k=-\infty}^{\infty} v_{rk} e^{jk\omega t} \quad (7)$$

where  $v_{tm}$  is the  $m$ th, and  $v_{rk}$  is the  $k$ th Fourier component of the terminal voltage and the voltage across the reactor. Note that for steady state operation, equal volt-seconds is always maintained across the reactor  $L_r$  so that the DC component of  $V_r(\omega t)$  is equal to zero.

The following relationship between the Fourier components of the reactor current and the reactor voltage can be obtained from (14):

$$\begin{bmatrix} \cdot \\ \cdot \\ I_{r-1} \\ I_{r0} \\ I_{r+1} \\ \cdot \\ \cdot \end{bmatrix} = \begin{bmatrix} \cdot & \cdot & \cdot & \cdot & \cdot & \cdot & \cdot \\ \cdot & \cdot & \frac{i}{-j\omega L_r} & 0 & 0 & \cdot & \cdot \\ \cdot & \cdot & \frac{e^{-j\phi_1}}{-j\omega L_r} & 0 & \frac{e^{j\phi_1}}{j\omega L_r} & \cdot & \cdot \\ \cdot & \cdot & 0 & 0 & \frac{1}{j\omega L_r} & \cdot & \cdot \\ \cdot & \cdot & \cdot & \cdot & \cdot & \cdot & \cdot \\ \cdot & \cdot & \cdot & \cdot & \cdot & \cdot & \cdot \end{bmatrix} \begin{bmatrix} \cdot \\ \cdot \\ v_{r-1} \\ 0 \\ v_{r+1} \\ \cdot \\ \cdot \end{bmatrix} \quad (15)$$

Rewriting (15) in short matrix form we obtain:

$$\mathbf{I}_r = \mathbf{Y}_r \mathbf{V}_r$$

$\mathbf{V}_r(\omega t)$  is the terminal voltage,  $\mathbf{V}_t(\omega t)$ , multiplied by the TCR switching function  $\mathbf{H}(\omega t)$ :

$$\mathbf{V}_r(\omega t) = \mathbf{V}_t(\omega t) \mathbf{H}(\omega t) \quad (16)$$

$\mathbf{V}_r(\omega t)$  can be thought of as an infinite vector of harmonic voltages, one for each harmonic frequency. Equation (16) can be expressed in matrix form as shown in (17). It is made up of an infinite dimensional switching function matrix  $\mathbf{H}$ , multiplied by the terminal voltage vector.

## Appendix B

### Harmonic Matrix of a Single Phase Bridge

This appendix derives the harmonic coupling matrix of the single phase bridge shown in the Figure B.1. The method is based on the switching functions shown in the Figure B.2.

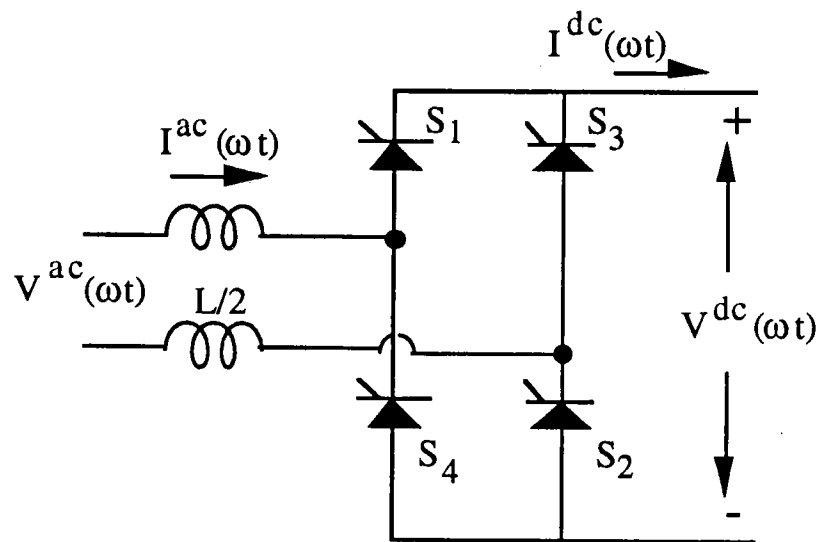


Figure B.1. Single phase line commutated converter

With the converter operating in the continuous mode,  $I^{ac}(\omega t)$  is essentially the sum of four separate current vectors corresponding to four different switching functions:

$$I^{ac}(\omega t) = I^1(\omega t) + I^3(\omega t) + I^{13}(\omega t) + I^{31}(\omega t) \quad (1)$$

Where:

$$I^1(\omega t) = (H^1(\omega t) - H^{13}(\omega t) - H^{31}(\omega t)) I^{ac}(\omega t),$$

$$I(\omega t) = \left( \int_{\phi_1}^{\omega t} \frac{V^{ac}}{\omega L} d\omega t \right) - I^{dc}(\phi_1) \quad (2)$$

where  $I^{dc}(\omega t = \phi_1)$  is the current in the circuit at the start of commutation. Therefore,  $I^{31}(\omega t)$  is given by:

$$I^{31}(\omega t) = H^{31}(\omega t) I(\omega t) \quad (3)$$

Assuming periodic operation, equation (3) can be written as:

$$\sum_{n=-\infty}^{\infty} I_n^{31} e^{jn\omega t} = \sum_{n,m=-\infty}^{\infty} h_n^{31}(\mu_1, \phi_1) * I_m e^{j(n+m)\omega t} \quad (4)$$

Where,

$$h_0^{31} = \frac{\mu_1}{2\pi} \quad (5)$$

$$h_{n \neq 0}^{31} = \frac{j}{2n\pi} e^{-jn\phi_1} [e^{-jn\mu_1} - 1] \quad (6)$$

The harmonic matrix form of equation (4) is shown in (7) and (8). It is made up of an infinite dimensional switching function  $H^{31}$  multiplied by the AC current vector  $I$ .

$$I^{31} = H^{31} I \quad (7)$$

$$\begin{bmatrix} \vdots \\ I_{-1} \\ I_0 \\ I_1 \\ \vdots \end{bmatrix} = \begin{bmatrix} \vdots \\ \frac{V_{-1}^{ac}}{-j\omega L} \\ 0 \\ \frac{V_1^{ac}}{-j\omega L} \\ \vdots \end{bmatrix} - \begin{bmatrix} \vdots \\ \dots 0 & 0 & 0 \dots \\ \dots e^{-j\phi_1} & 1 & e^{j\phi_1} \dots \\ \dots 0 & 0 & 0 \dots \\ \vdots \end{bmatrix} \begin{bmatrix} \vdots \\ I_{-1}^{dc} + \frac{V_{-1}^{ac}}{-j\omega L} \\ I_0^{dc} \\ I_1^{dc} + \frac{V_1^{ac}}{-j\omega L} \\ \vdots \end{bmatrix} \quad (12)$$

The short matrix form of equation (12) can be written as:

$$\mathbf{I} = \mathbf{Y} \mathbf{V}^{ac} - \mathbf{G}(\phi_1) [\mathbf{I}^{dc} + \mathbf{Y} \mathbf{V}^{ac}] \quad (13)$$

Note that the presence of the term  $\{-\mathbf{G}(\phi_1) [\mathbf{I}^{dc} + \mathbf{Y} \mathbf{V}^{ac}]\}$  in (13) ensures the current vector  $(\mathbf{Y} \mathbf{V}^{ac})$  is initialized to the DC current just before the start of the commutation process. Equation (7) for  $\mathbf{I}^{31}$  now can be written as;

$$\mathbf{I}^{31} = \mathbf{H}^{31} [\mathbf{Y} \mathbf{V}^{ac} - \mathbf{G}(\phi_1) [\mathbf{I}^{dc} + \mathbf{Y} \mathbf{V}^{ac}]] \quad (14)$$

A similar argument can be used to find the AC current in the commutation time frame of  $\mathbf{H}^{31}$  as:

$$\mathbf{I}^{13} = \mathbf{H}^{13} [\mathbf{Y} \mathbf{V}^{ac} - \mathbf{G}(\phi_2) [\mathbf{I}^{dc} - \mathbf{Y} \mathbf{V}^{ac}]] \quad (15)$$

Inspection of the circuit shown in Figure B.1 allows us to compute the time functions  $I^1(\omega t)$  and  $I^3(\omega t)$  as follows:

$$I^1(\omega t) + I^3(\omega t) = (H^1(\omega t) - H^3(\omega t)) I^{dc}(\omega t) \quad (16)$$



## Appendix C

### TCR Current Harmonics of the Example 5.3

During the early design phase of the 230KV, 330 Mvar ASC system near the Kayenta substation a "second resonance" was found which resulted in doubling the size of the thyristor control reactor to remove this "resonance". In chapters 5.3 and 5.4, both the initial and the final design of the Kayenta system were analyzed. This appendix shows the TCR current harmonics for the three possible values of the thyristor control reactor, namely 1.7 mH, 3.4 mH (initial design) and 6.8 mH (final design).

Figures C.1a, C.1c and C.1e show the fundamental component of the TCR. Similarly, Figures C.1b, C.1d and C.1f show the 3rd component of the TCR current. These harmonic currents are plotted as a function of the requested value for the thyristor conduction time  $\sigma_p$ . Only the periodic orbits which are half wave symmetric are shown so that  $\sigma_1 = \sigma_2 = \sigma_p$ . All the plots are normalized to the fundamental component  $\sigma_p = 180^\circ$ . In addition to the expected fundamental resonance, the system with the  $L_r$  values 1.7 mH or 3.4 mH also predict the unexpected "second resonance" region. This region does not have any half wave symmetric periodic solutions. Moreover, as  $\sigma_p$  is decreased from  $180^\circ$  towards this region, a rapid 3rd harmonic current build up as seen. Note that the previously predicted 3rd harmonic resonance points from the average inductor model fall within the shaded regions for both cases.

## Appendix D

### DC and AC Harmonics of the Example 7.3

This appendix presents the results of the classical method versus the harmonic coupling approach for the example system described in chapter 7.3. The results are plotted versus the commutation time  $\mu$  and correspond to the inverter DC and AC harmonic currents and voltages.

Figure D.1a shows harmonic contents of the inverter AC current. All of the current harmonics are normalized to the fundamental current when  $\mu \cong 58^\circ$ . In region B, as  $\mu$  increases, all the odd harmonics become very large.

Figure D.1b shows harmonic contents of the inverter AC voltage. The AC voltage harmonics are normalized to the no load AC bus voltage. The 3rd harmonic is very small due to the presence of the passive tuned filter in the example system.

Figure D.2a shows harmonic contents of the inverter DC current. The DC side harmonic currents are normalized to the average of the DC current when  $\mu \cong 58^\circ$ .

Figure D.2b shows harmonic contents of the inverter DC voltage. All of the plots are normalized to the average of the DC voltage when  $\mu \cong 58^\circ$ . The region B shows a peculiar drop of the 2nd harmonic voltage on the DC side. However, both of the regions show large harmonics as periodic solutions of the system approach the shaded region.

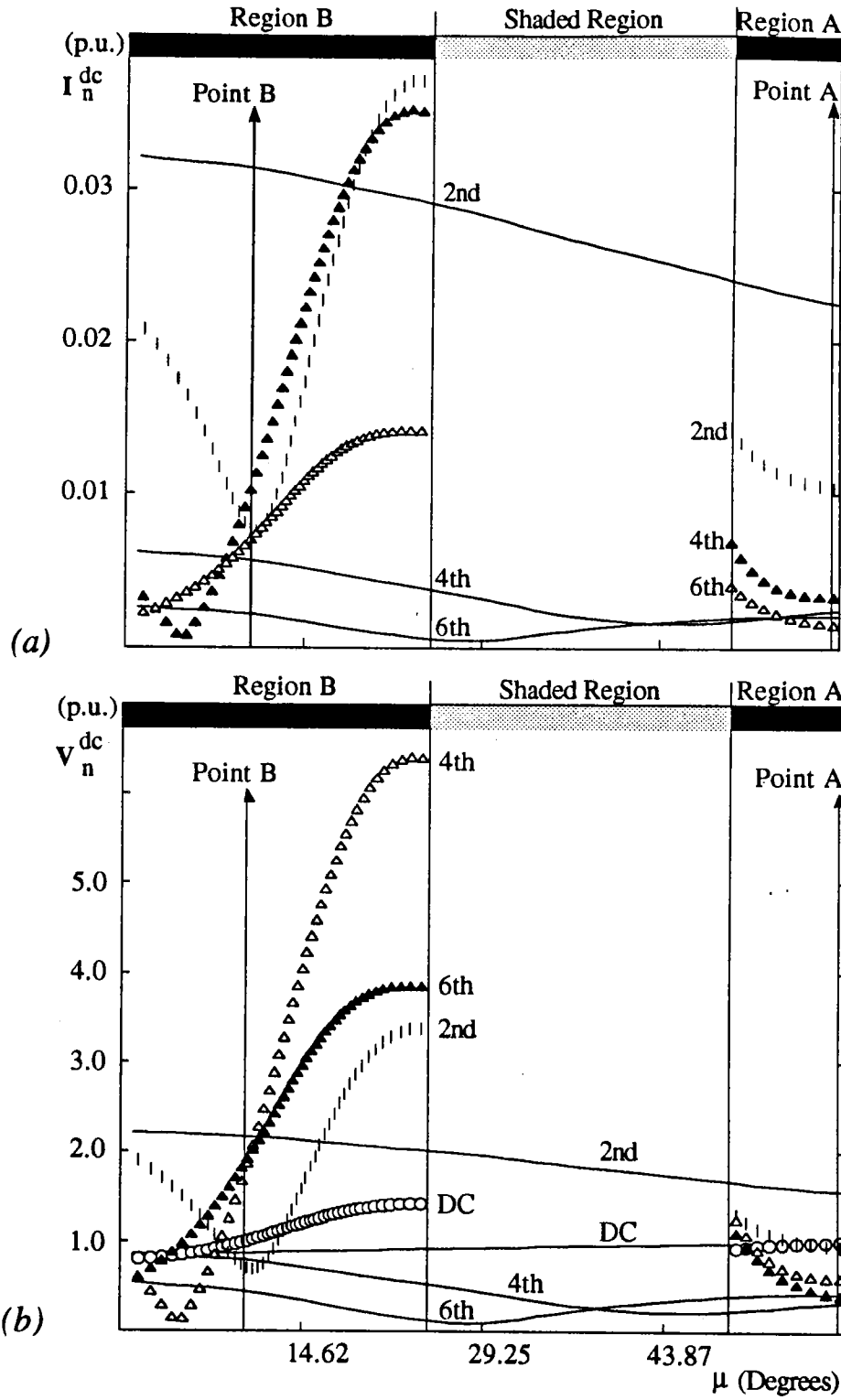


Figure D.2. DC harmonics of the example 7.3 (a) current (b) voltage

## References

- [1] J.D. Ainsworth, "Harmonic instability between controlled static converters and ac networks," Proc. Inst. Elec. Eng., Vol. 114, pp. 949-957, July 1967
- [2] P.M. Anderson, B.L. Agrawal, J.E. Van Ness, Subsynchronous Resonance in Power Systems, IEEE Press, New York, 1990.
- [3] H. D'Angelo, "Linear Time-Varying Systems: Analysis and Synthesis," Allyn and Bacon, Boston, Mass., Ch. 7, 1970.
- [4] J. Arrillaga, High voltage direct current transmission, Peter Peregrinus Ltd., London, UK.
- [5] F.M. Arscott, "Periodic Differential Equations," The MacMillan Co., New York, New York, 1975.
- [6] J.W. Ballance and Goldberg, "Subsynchronous resonance in series compensated transmission lines", IEEE Transactions on Power Apparatus and Systems, Vol. PAS-92, pp. 1649-1658, September-October 1973.
- [7] L.J. Bohmann, R.H. Lasseter; "Harmonic Interactions in Thyristor Controlled Reactor Circuits", IEEE Transactions on Power Delivery, Vol. 4, No. 3, pp. 1919-1926 July 1989.

- [14] H.W. Dommel, "Digital Computer Solution of Electromagnetic Transients in Single and Multiphase Networks," IEEE Transactions on Power Apparatus and Systems, VOL. PAS-88, pp. 388-399, April 1969
- [15] Electromagnetic Transients Program; Workbook 4, EPRI EL - 4151 Volume 4, June 1989.
- [16] K.A. Ellithy and M.A. Choudhry, "Effect of load models on AC/DC system stability and modulation control design", IEEE Trans. on Power Systems, May 1989 pp. 411-417.
- [17] L.E. Eilts, "Flexible AC Transmission system projects of western area power administration", Current Activity in Flexible AC Transmission Systems April 92 pp.17-19.
- [18] D.N. Ewart, R.J. Koessler, et. al., "Investigation of Facts Options to Utilize the Full Thermal Capacity of AC Transmission," a paper presented at the first Flexible AC Transmission Systems (FACTS) conference, Cincinnati, Ohio, Nov. 14-16 1990.
- [19] M. Grotzbach and R.V. Lutz, "Unified modelling of rectifier controlled DC power supplies", IEEE Trans. on Power Electronics, Vol 1, No 2, April 1986, pp. 90-100.
- [20] J. Guckenheimer, P. Holmes, Nonlinear oscillations, dynamical systems and bifurcations of vector fields, Springer-Verlag, NY, 1986.

- [28] E. Larsen, C. Bowler, B. Damsky and S. Nilsson, "Benefits of Thyristor-Controlled Series Compensation," Cigre paper 14/37/38-04, Paris 1992.
- [29] J.P. Louis, "Nonlinear and linearized models for control systems including static convertors, Third IFAC Symposium on control on power electronics and electrical derives, Lausanne, Switzerland, Sept. 1983, pp. 9-16.
- [30] W. MacMurray, "Stability theory of convertors with counter EMF load," in Proc U.S. Japan Conference S5.1, 1981, pp. 159-168
- [31] W. Magnus and S. Winkler, "Hill's Equation," John Wiley and Sons, NewYork, NewYork, 1966.
- [32] R.M. Maliszewski, B.M. Pasternack, et. al., "Power Flow Control in a Highly Integrated Transmission Network," Cigre paper 37-303, Paris 1990.
- [33] N. Martins and L.T.G. Lima, "Determination of suitable locations for power system stabilizers and static VAR compensators for damping electromechanical oscillations in large scale power system", IEEE Trans. on Power Systems, Nov. 1990, pp. 1455-1463.
- [34] R.D. Middlebrook and S. Cuk, "A general unified approach to modelling switching power converter stage", IEEE Power Electronics Specialists Conference, 1976, pp.18-34.

Networks," Presented at the IEEE/PES 1991 Winter Meeting, New York, New York, February 3-7, 1991.

- [42] R. P. Stratford, "Analysis and Control of Harmonic Current in Systems with Static Power Converters," The IEEE Transactions on Industry Applications, VOL. IA-17, NO. 1, Jan./Feb. 1981.
- [43] R. P. Stratford, "Rectifier Harmonics in Power Systems," IEEE Transactions on Industry Applications, Vol. IA-16, No. 2, March/April 1980.
- [44] Subsynchronous Resonance Working Group of the System Dynamic Performance Subcommittee, "Reader's Guide to subsynchronous resonance", IEEE Trans. on Power Systems, Vol 7, No. 1, Feb. 1992, pp. 150-157.
- [45] F.D. Tan, R.S. Ramshaw, "Instabilities of a boost converter system under large parameter variations", IEEE Transactions on Power electronics, vol. 4, no 4, October 1989, pp. 442-459.
- [46] J.M.T. Thompson, H.B. Stewart, "Nonlinear Dynamics and chaos: geometrical methods for scientists and engineers", John Wiley, London, 1986, reprinted 1987.
- [47] G.C. Verghese, M.E. Elbuluk, J.G. Kassakian, "A General Approach to sampled-data modelling for power electronic circuits", IEEE Transactions on Power Electronics, Vol 1, No 2, April 86, pp. 76-89.